NeuroImage 146 (2017) 171–187

Contents lists available at ScienceDirect

NeuroImage

journal homepage: www.elsevier.com/locate/neuroimage

Robustness and dynamicity of functional networks in phantom sound

Anusha Mohan [a], Dirk De Ridder [b], Sven Vanneste [a,*]

[a] Lab for Clinical & Integrative Neuroscience, School of Behavioral and Brain Sciences, The University of Texas at Dallas, USA
[b] Department of Surgical Sciences, Section of Neurosurgery, Dunedin School of Medicine, University of Otago, Dunedin, New Zealand

ARTICLE INFO

Article history:
Received 14 December 2015
Accepted 14 April 2016
Available online 18 April 2016

Keywords:
Tinnitus
EEG
Multimodal
Rich-club
Damage-modeling

ABSTRACT

Phantom sound perception is the perception of a sound in the absence of a corresponding external sound source. It is a common symptom for which no treatment exists. Gaining a better understanding of its pathophysiology by applying network science might help in identifying targets in the brain for neuromodulatory approaches to treat this elusive symptom. Brain networks are commonly organized as functional modules which have a densely connected core network coupled to a communally-organized peripheral network. The core network is called the rich club network and the peripheral network is divided into the feeder and local networks. In current study, we investigate the effects of virtual lesions on the endogenous dynamics, complexity and robustness of the remaining brain. It is hypothesized that depending on whether nodes is functionally central to the network or not, the robustness and dynamics of the network change when a lesion in introduced. We therefore investigate the effect of introducing a virtual focal lesion randomly to different nodes is in the tinnitus network and contrast it to the effect of specifically targeting the nodes of the rich-club, feeder and local nodes in patients experiencing a phantom sound (i.e. tinnitus). The tinnitus and control networks were computed from the source-localized EEG of 311 tinnitus patients and 256 control subjects. The results of the current study indicate that both the tinnitus and control networks are robust to the attack on random and rich club nodes, but are drastically modified when attacked from the periphery, especially while targeting the feeder hubs. In both the tinnitus and control networks, feeder nodes were found to have a higher betweenness centrality value than the rich club nodes. This shows that the feeders have a larger influence on the information transmission through the brain than the rich club nodes, by transferring information from the peripheral communities to the core. Further, evidence for the theoretical model of a multimodal tinnitus network is also presented showing that the tinnitus network is divided into individual, separable modules each possibly encoding a different aspect of tinnitus. The current study alludes to the concept that the efficient modification of the tinnitus network is theoretically possible by disconnecting the individual communities from the core of the pathological network.

1. Introduction

Application of network connectomics has spanned a vast majority of domains such as social (Duncan J. Watts, 1999), computer (Strogatz, 2001), protein (Wuchty, 2001) and brain networks (Danielle Smith Bassett and Bullmore, 2006). According to graph theory, these networks are structured into a "small-world" topology (Duncan J. Watts, 1999; D. J. Watts and Strogatz, 1998) within which individual nodes connect to each other and a small proportion of nodes, called hubs, facilitate long-distance connectivity (D. S. Bassett et al., 2008). This has become a widely accepted model for complex systems because it accounts for an economic balance between network efficiency and the structural cost of wiring the system (Sophie Achard and Bullmore, 2007; Danielle Smith Bassett and Bullmore, 2006; Bullmore and Sporns, 2012; Strogatz, 2001; Duncan J. Watts, 1999). The robustness of such functional networks has been investigated in a number of complex systems (Albert et al., 2000; Doyle et al., 2005), including biological networks (Alstott et al., 2009; Jeong et al., 2001). From a network perspective, changes in brain dynamics as a result of acute injuries such as trauma, tumor, or stroke, as well as chronic or degenerative disturbances, correspond to node and edge deletions in the brain connectome (Alstott et al., 2009). Conversely, in the current study, we investigate the effects of theoretically inducing focal lesions (by removing a set of spatially localized nodes) on the endogenous dynamics, complexity and robustness of the remaining brain.

Networks can be further described as having a community structure (Flake et al., 2002; Fortunato, 2010), a core-periphery structure (Holme, 2005; Rombach et al., 2014) or a combination of the two (Yang and Leskovec, 2014). Community structures have been

* Correspondence to: Lab for Clinical & Integrative Neuroscience, School of Behavioral & Brain Sciences, University of Texas at Dallas, W 1966, Inwood Rd, Dallas, Texas 75235, USA.
E-mail addresses: sven.vanneste@utdallas.edu (S. Vanneste).
URL: http://www.lab-clint.org (S. Vanneste).

http://dx.doi.org/10.1016/j.neuroimage.2016.04.033
1053-8119/

Table 1
Characteristics of tinnitus patients.

Ear	
Unilateral	114
Bilateral	197
Tone	
Pure tone	118
Noise Like	193
TQ	
Mean	39.37
SD	17.59
Tinnitus frequency (Hz)	
Mean	5143
SD	3183
Tinnitus loudness (dB SL)	
Mean	7.85
SD	8.78

characterized to typically consist of densely populated, specialized modules that are functionally integrated through sparse inter-modular connections (Fortunato, 2010). On the other hand, a core-periphery based structure is cemented on a foundational core network which branches outwardly into a diffuse peripheral network (Rombach et al., 2014). However, the core may or may not be central to the network as a whole (Holme, 2005). A combination of community and core-periphery structures has been shown to materialize into a multimodal network with overlapping communities (Yang and Leskovec, 2014). This results in a network having a densely connected core which is coupled to an organized peripheral network. Such a structure has been extensively studied in brain networks as the "rich-club" connectome (Bullmore and Sporns, 2012; M. P. van den Heuvel and Sporns, 2011). The peripheral network in a "rich-club" connectome further consists of a feeder network which provides direct input to the rich club nodes and a local network consisting of connections between non rich-club nodes (M. P. van den Heuvel and Sporns, 2011; Martijn P. van den Heuvel and Sporns, 2013). The feeder nodes along with the rich club nodes are responsible for inter-modular connections and the local network is responsible for intra-modular connections.

The current study aims to investigate the robustness of functional brain networks to virtual focal lesions and presents empirical evidence for a multimodal network organization that is disorder specific. This involves the removal of nodes at random or in association with a certain network parameter (nodes with high betweenness centrality or belonging to the rich club, feeder or local networks). We focus on the cortical differences in resting-state, eyes-closed, source localized EEG between tinnitus patients and healthy controls. Tinnitus or phantom sound is the perception of a sound in the absence of a corresponding external auditory stimulus. It is a common symptom for which no treatment exists (Langguth et al., 2013). Gaining a better understanding of its pathophysiology by applying network science might provide an empirical tool for identifying targets in the brain for effective neuromodulation of this elusive symptom. Tinnitus is a complex functional disorder which is characterized by multiple components such as pitch, loudness, associated mood and distress changes, laterality, type (noise-like, pure tone) etc. (De Ridder et al.,

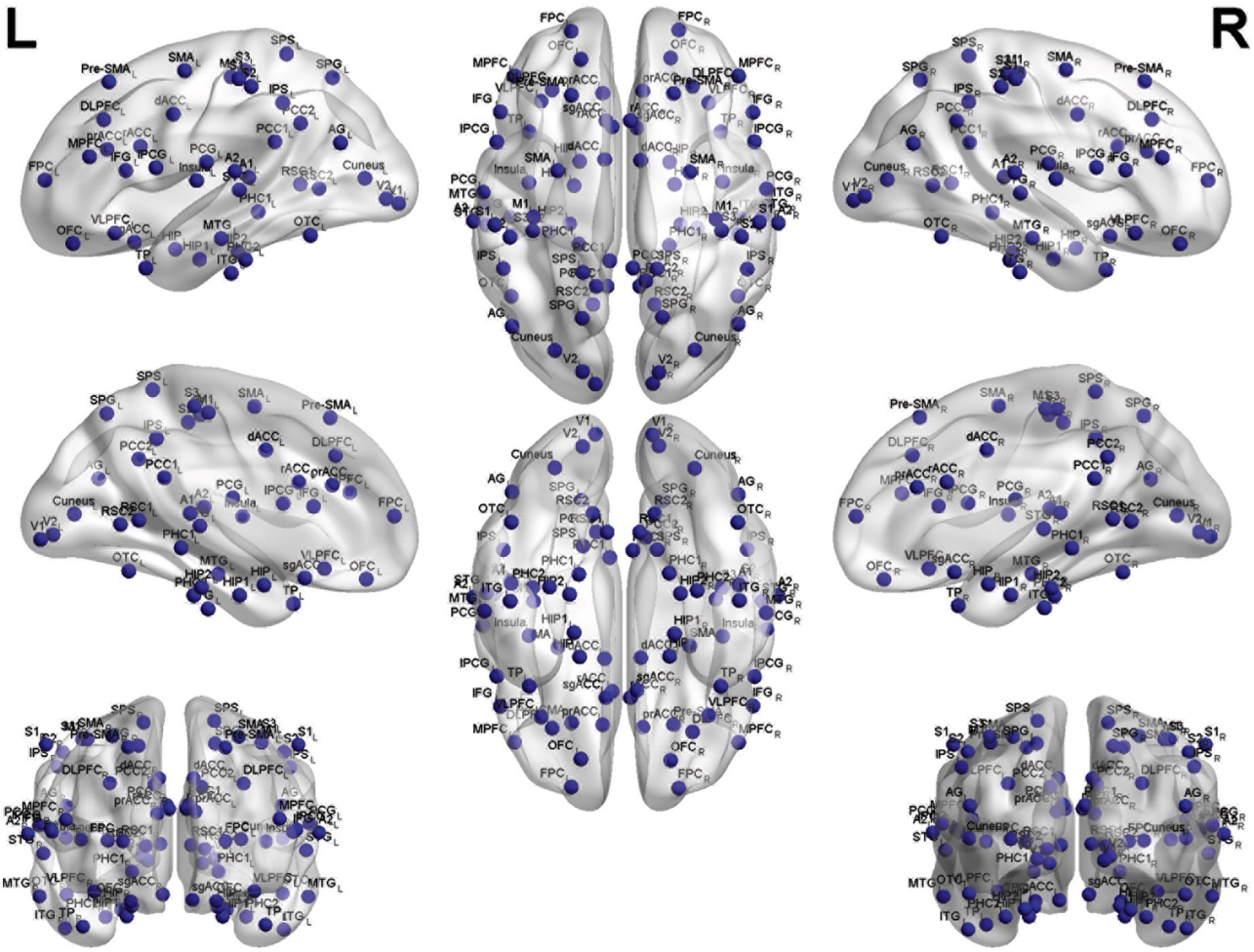

Fig. 1. All the Brodmann areas included in the study.

Table 2
All the Brodmann areas included in the study.

Brodmann areas	Abbreviation	Name of the brodmann area
BA01	S1	Primary somatosensory cortex
BA02	S2	Secondary somatosensory cortex
BA03	S3	Tertiary somatosensory cortex
BA04	M1	Primary motor cortex
BA05	SPS	Superior parietal sulcus
BA06	SMA	Supplementary motor area
BA07	SPG	Superior parietal gyrus
BA08	Pre-SMA	Pre-supplementary motor area
BA09	DLPFC	Dorsolateral prefrontal cortex
BA10	FPC	Fronto-parietal cortex
BA11	OFC	Orbital frontal cortex
BA13	Insula	Insula
BA17	V1	Primary visual cortex
BA18	V2	Secondary visual cortex
BA19	Cuneus	Cuneus
BA20	ITG	Inferior temporal gyrus
BA21	MTG	Medial temporal gyrus
BA22	STG	Superior temporal gyrus
BA23	PCC1	Posterior cingulate cortex1
BA24	dACC	Dorsal anterior cingulate cortex
BA25	sgACC	Subgeneual anterior cingulate cortex
BA27	PHC1	Parahippocampal gyrus1
BA28	HIP1	Hippocampal area1
BA29	RSC1	Retrosplinal cortex1
BA30	RSC2	Retrosplinal cortex2
BA31	PCC2	Posterior cingulate cortex2
BA32	prACC	pregeneual anterior cingulate cortex
BA33	rACC	Rostral anterior cingulate cortex
BA34	HIP	Hippocampus
BA35	HIP2	Hippocampal area2
BA36	PHC2	Parahippocampal gyrus2
BA37	OTC	Occipital-temporal cortex
BA38	TP	Temporal pole
BA39	AG	Angular gyrus
BA40	IPS	Intra-parietal sulcus
BA41	A1	Primary auditory cortex
BA42	A2	Secondary auditory cortex
BA43	PCG	Postcentral gyrus
BA44	OPCG	Opercular part of inferior frontal gyrus
BA45	IFG	Inferior frontal gyrus
BA46	MPFC	Medial prefrontal cortex
BA47	VLPFC	Ventero-lateral prefrontal cortex

2014a, 2014b). Recently, tinnitus was hypothesized to be the result of multiple separable but overlapping sub-networks each encoding a different component of the disorder, but integrated into a unified phantom percept by overlapping hubs (De Ridder et al., 2014a, 2014b). Conceptually the hubs could be interconnected to form a rich club, binding and integrating information from the different subnetworks. The computational complex-network approach taken in this paper will provide a new link between localized changes of brain networks and global disruptions of dynamic interactions. This will help us confirm that the unified tinnitus percept is indeed an emergent property of a multimodal network with specialized modules that are functionally integrated through sparse inter-modular connections. Analysis of resting state data has the advantage that it looks at the endogenous dynamics of neurophysiological processes. The results might theoretically determine the most effective targets for invasive or non-invasive neuromodulation. This is of particular interest to tinnitus, since there is no cure for this disorder as of today.

Table 3
Thresholds and number of undirected edges.

Frequency	Threshold in controls	Number of edges in controls	Threshold in tinnitus	Number of edges in tinnitus
Delta	.0155	2053	.0095	2048
Theta	.026	2006	.0104	2003
Alpha1	.07	2016	.0545	2008
Alpha2	.051	2131	.033	2107
Beta1	.019	2011	.0227	2010
Beta2	.017	2102	.0195	2112
Beta3	.006	1984	.0107	1982
Gamma	.005	2093	.0065	2100

2. Materials and methods

2.1. Patients with an auditory phantom percept

The patient sample consisted of 311 patients ($M = 50.63$ years; $SD = 13.67$; 210 males and 101 females) everyone experiencing continuous tinnitus. The patient's condition was considered chronic if the onset of the tinnitus dated back a year or more. The homogeneity of the sample was increased by excluding individuals with pulsatile tinnitus, Ménière disease, otosclerosis, chronic headache, neurological disorders such as brain tumors, and individuals being treated for mental disorders. The perceived location of patients' tinnitus (the left ear, in both ears, and centralized in the middle of the head (bilateral), the right ear) as well the type of tinnitus (pure tone-like tinnitus or noise-like tinnitus) was noted. Audiometric tests consisted of pure tone audiometry, where

Table 4
List of Rich Club nodes in the eight frequency bands:

Frequency bands	Tinnitus	Controls
Delta	*Left*: PHC1, PHC2, IPS, S2, RSC2 *Right*: PCG, STG, A1, A2, S2, S3, M1, MTG2, Cuneus, OTC	*Left*: Pre-SMA, OTC, IPCG, DLPFC, TP, IFG *Right*: Pre-SMA, SPS, S1, S2, S3, M1, DLPFC
Theta	*Left*: RSC1, RSC2, PHC1, PHC2, HIP2, OTC, V1, V2, PCC1 *Right*: SMA, PCC1	*Left*: rACC, Pre-SMA, DLPFC, sgACC *Right*: SMA, S1, S2, S3, IPS, M1, sgACC, rACC
Alpha1	*Left*: V1, V2, Cuneus, ITG, RSC1, RSC2, OTC, PCC1, PHC1, PHC2, MTG, HIP1, HIP2 *Right*: V1, V2, Insula, MTG, SPS, ITG, RSC1, RSC2, HIP, HIP1, PCC1, PCC2, SMA	*Left*: S1, S2, S3, M1, SPS, SMA, SPG, Pre-SMA, FPC, Insula, V1, V2, Cuneus, ITG, MTG, STG, PCC1, PCC2, dACC, PHC1, PHC2, RSC1, RSC2, HIP, HIP1, HIP2, prACC, OTC, TP, AG, IPS, A1, A2, PCG, DLPFC, OFC, rACC, IPCG, VLPFC, sgACC, IFG, MPFC *Right*: Same as left
Alpha2	*Left*: IPS, S1, S2, S3, ITG, A1, OTC, V1, Cuneus, HIP1, PHC2, AG, M1, MTG *Right*: SPS, V1, V2, S1, S2, S3, M1, Cuneus	*Left*: Cuneus, OTC, V1, V2 *Right*: IPS, OTC, A1, A2, AG, V1, S2
Beta1	*Left*: V1, V2, Cuneus, RSC2, sgACC *Right*: V1, V2, OFC, sgACC	*Left*: Insula, RSC1, RSC2, V1, V2, M1, sgACC, PCG, MTG, PHC1, PHC2, S1, S2, S3, HIP, HIP1. HIP2, ITG, STG, OTC, A1, A2, IPCG, OFC, TP *Right*: RSC1, RSC2, V1, Cuneus, AG, PCC1, PCC2, sgACC
Beta2	*Left*: FPC, V1, V2 *Right*: VLPFC, HIP, HIP1, Pre-SMA, V1, sgACC	*Left*: Insula, dACC, PCG, HIP, HIP1, HIP2, ITG, MTG, IPCG, A2, STG *Right*: dACC, HIP, HIP1
Beta3	*Left*: sgACC, SPS, Pre-SMA, rACC, DLPFC, dACC, prACC *Right*: Pre-SMA, DLPFC, MTG, HIP, HIP1, dACC, sgACC, rACC, Insula, IPCG	*Left*: PCC1, ITG, RSC1 *Right*: RSC1, RSC2, PHC1, Pre-SMA, dACC, PCC1, PCC2, SPS
Gamma	*Left*: SMA, M1, dACC, S3, PCC1, PCC2, SPS *Right*: dACC, M1, S3, SPS, PCC1, PCC2	*Left*: dACC, SMA, Pre-SMA, rACC, PCC1, prACC *Right*: dACC, Pre-SMA, DLPFC, M1, rACC, SMA, SPS, PCC2, S3

Table 5
List of feeder nodes in the eight frequency bands.

Frequency bands	Tinnitus	Controls
Delta	*Left*: S1, S3, M1, SPS, SMA, SPG, Pre-SMA, FPC, Insula, V1, V2, Cuneus, ITG, MTG, STG, PCC1, PCC2, dACC, RSC1, HIP, HIP1, HIP2, prACC, OTC, TP, AG, A1, A2, PCG, DLPFC, OFC, rACC, IPCG, VLPFC, sgACC, IFG, MPFC *Right*: S3, SPS, SMA, SPG, Pre-SMA, FPC, Insula, V1, V2, ITG, PCC1, PCC2, dACC, PHC1, PHC2, RSC1, RSC2, HIP, HIP1, HIP2, prACC, TP, AG, IPS, DLPFC, OFC, rACC, IPCG, VLPFC, sgACC, IFG, MPFC	*Left*: S1, S2, S3, M1, SPS, SMA, SPG, FPC, Insula, V1, V2, Cuneus, ITG, MTG, STG, PCC1, PCC2, dACC, PHC1, PHC2, RSC1, RSC2, HIP, HIP1, HIP2, prACC, AG, IPS, A1, A2, PCG, OFC, rACC, VLPFC, sgACC, MPFC *Right*: SMA, SPG, FPC, Insula, V1, V2, Cuneus, ITG, MTG, STG, PCC1, PCC2, dACC, PHC1, PHC2, RSC1, RSC2, HIP, HIP1, HIP2, prACC, OTC, TP, AG, IPS, A1, A2, PCG, OFC, rACC, IPCG, VLPFC, sgACC, IFG, MPFC
Theta	*Left*: S1, S2, S3, M1, SPS, SMA, SPG, Pre-SMA, FPC, Insula, ITG, MTG, STG, PCC2, dACC, HIP, HIP1, prACC, TP, AG, IPS, A1, A2, PCG, DLPFC, OFC, rACC, IPCG, VLPFC, sgACC, IFG, MPFC *Right*: S1, S2, S3, M1, SPS, SPG, Pre-SMA, FPC, Insula, V1, V2, Cuneus, ITG, MTG, STG, PCC2, dACC, PHC1, PHC2, RSC1, RSC2, HIP, HIP1, HIP2, prACC, OTC, TP, AG, IPS, A1, A2, PCG, DLPFC, OFC, rACC, IPCG, VLPFC, sgACC, IFG, MPFC	*Left*: S1, S2, S3, M1, SPS, SMA, SPG, FPC, Insula, V1, V2, Cuneus, ITG, MTG, STG, PCC1, PCC2, dACC, PHC1, PHC2, RSC1, RSC2, HIP, HIP1, HIP2, prACC, OTC, TP, AG, IPS, A1, A2, PCG, OFC, IPCG, VLPFC, IFG, MPFC *Right*: S3, SPS, SPG, Pre-SMA, FPC, Insula, V1, V2, Cuneus, ITG, MTG, STG, PCC1, PCC2, dACC, PHC1, PHC2, RSC1, RSC2, HIP, HIP1, HIP2, prACC, OTC, TP, AG, A1, A2, PCG, DLPFC, OFC, IPCG, VLPFC, IFG, MPFC
Alpha1	*Left*: S1, S2, S3, M1, SPS, SMA, SPG, Pre-SMA, FPC, Insula, STG, PCC2, dACC, HIP, prACC, TP, AG, IPS, A1, A2, PCG, OFC, rACC, IPCG, VLPFC, sgACC, IFG, MPFC *Right*: S1, S2, S3, M1, SPG, Pre-SMA, FPC, Cuneus, dACC, PHC1, PHC2, HIP2, prACC, OTC, TP, AG, IPS, A1, A2, PCG, OFC, rACC, IPCG, VLPFC, sgACC	No feeder nodes identified
Alpha2	*Left*: SPS, SMA, SPG, Pre-SMA, FPC, Insula, V2, STG, PCC1, PCC2, dACC, PHC1, RSC1, RSC2, HIP, HIP2, prACC, TP, A2, PCG, DLPFC, OFC, rACC, IPCG, VLPFC, sgACC, IFG, MPFC *Right*: SMA, SPG, Pre-SMA, FPC, Insula, ITG, MTG, STG, PCC1, PCC2, dACC, PHC1, PHC2, RSC1, RSC2, HIP, HIP1, HIP2, OTC, TP, AG, IPS, A1, A2, PCG, DLPFC, OFC, rACC, IPCG, VLPFC, sgACC, IFG, MPFC	*Left*: S1, S2, S3, M1, SPS, SMA, SPG, Pre-SMA, FPC, Insula, ITG, MTG, STG, PCC1, PCC2, dACC, PHC1, PHC2, RSC1, RSC2, HIP, HIP1, HIP2, prACC, TP, AG, IPS, A1, A2, PCG, DLPFC, OFC, rACC, IPCG, VLPFC, sgACC, IFG, MPFC *Right*: S1, S3, M1, SPS, SMA, SPG, Pre-SMA, FPC, Insula, V2, Cuneus, ITG, MTG, STG, PCC1, PCC2, dACC, PHC1, PHC2, RSC1, RSC2, HIP, HIP1, HIP2, prACC, TP, PCG, DLPFC, OFC, rACC, IPCG, VLPFC, sgACC, IFG, MPFC
Beta1	*Left*: S1, S2, S3, M1, SPS, SMA, SPG, Pre-SMA, FPC, Insula, ITG, MTG, STG, PCC1, PCC2, dACC, PHC1, PHC2, RSC1, HIP, HIP1, HIP2, prACC, OTC, TP, AG, IPS, A1, A2, PCG, DLPFC, OFC, rACC, IPCG, VLPFC, IFG, MPFC *Right*: S1, S2, S3, M1, SPS, SMA, SPG, Pre-SMA, FPC, Insula, Cuneus, ITG, MTG, STG, PCC1, PCC2, dACC, PHC1, PHC2, RSC1, RSC2, HIP, HIP1, HIP2, prACC, OTC, TP, AG, IPS, A1, A2, PCG, DLPFC, rACC, IPCG, VLPFC, IFG, MPFC	*Left*: S1, S2, S3, M1, SPS, SPG, FPC, Insula, V1, V2, Cuneus, ITG, MTG, STG, PCC2, PHC1, PHC2, RSC1, RSC2, HIP, HIP1, HIP2, OTC, TP, AG, IPS, A1, A2, PCG, DLPFC, OFC, IPCG, VLPFC, sgACC, IFG, MPFC *Right*: S1, S2, SPG, FPC, Insula, V1, V2, Cuneus, ITG, MTG, STG, PHC1, PHC2, RSC1, RSC2, HIP, HIP1, HIP2, OTC, TP, AG, IPS, A1, A2, PCG, OFC, sgACC
Beta2	*Left*: S1, S2, S3, M1, SPS, SMA, SPG, Pre-SMA, Insula, Cuneus, ITG, MTG, STG, PCC1, PCC2, dACC, PHC1, PHC2, RSC1, RSC2, HIP, HIP1, HIP2, prACC, OTC, TP, AG, IPS, A1, A2, PCG, DLPFC, OFC, rACC, IPCG, VLPFC, sgACC, IFG, MPFC *Right*: S1, S2, S3, M1, SPS, SMA, SPG, FPC, Insula, V2, Cuneus, ITG, MTG, STG, PCC1, PCC2, dACC, PHC1, PHC2, RSC1, RSC2, HIP2, prACC, OTC, TP, AG, IPS, A1, A2, PCG, DLPFC, OFC, rACC, IPCG, IFG, MPFC	*Left*: S1, S2, S3, M1, SPS, SMA, SPG, Pre-SMA, FPC, V1, V2, Cuneus, PCC1, PCC2, PHC1, PHC2, RSC1, RSC2, prACC, OTC, TP, AG, IPS, A1, DLPFC, OFC, rACC, VLPFC, sgACC, IFG, MPFC *Right*: S1, S2, S3, M1, SPS, SMA, SPG, Pre-SMA, FPC, Insula, V1, V2, Cuneus, ITG, MTG, STG, PCC1, PCC2, PHC1, PHC2, RSC1, RSC2, HIP2, prACC, OTC, TP, AG, IPS, A1, A2, PCG, DLPFC, OFC, rACC, IPCG, VLPFC, sgACC, IFG, MPFC
Beta3	*Left*: S1, S2, S3, M1, SMA, SPG, FPC, Insula, V1, V2, Cuneus, ITG, MTG, STG, PCC1, PCC2, PHC1, PHC2, RSC1, RSC2, HIP, HIP1, HIP2, OTC, TP, AG, IPS, A1, A2, PCG, OFC, IPCG, VLPFC, IFG, MPFC *Right*: S1, S2, S3, M1, SPS, SMA, SPG, FPC, V1, V2, Cuneus, ITG, STG, PCC1, PCC2, PHC1, PHC2, RSC1, RSC2, HIP2, prACC, OTC, TP, AG, IPS, A1, A2, PCG, OFC, VLPFC, IFG, MPFC	*Left*: S1, S2, S3, M1, SPS, SMA, SPG, Pre-SMA, FPC, Insula, V1, V2, Cuneus, MTG, STG, PCC2, dACC, PHC1, PHC2, RSC2, HIP, HIP1, HIP2, prACC, OTC, TP, AG, IPS, A1, A2, PCG, DLPFC, OFC, rACC, IPCG, VLPFC, sgACC, IFG, MPFC *Right*: S1, S2, S3, M1, SMA, SPG, FPC, Insula, V1, V2, Cuneus, ITG, MTG, STG, PHC2, HIP, HIP1, HIP2, prACC, OTC, TP, AG, IPS, A1, A2, PCG, DLPFC, OFC, rACC, IPCG, VLPFC, sgACC, IFG, MPFC
Gamma	*Left*: S1, S2, SPG, Pre-SMA, FPC, Insula, V1, V2, Cuneus, ITG, MTG, STG, PHC1, PHC2, RSC1, RSC2, HIP, HIP1, HIP2, prACC, OTC, TP, AG, IPS, A1, A2, PCG, DLPFC, OFC, rACC, IPCG, VLPFC, sgACC, IFG, MPFC *Right*: S1, S2, SMA, SPG, Pre-SMA, FPC, Insula, V1, V2, Cuneus, ITG, MTG, STG, PHC1, PHC2, RSC1, RSC2, HIP, HIP1, HIP2, prACC, OTC, TP, AG, IPS, A1, A2, PCG, DLPFC, OFC, rACC, IPCG, VLPFC, sgACC, IFG, MPFC	*Left*: S1, S2, S3, M1, SPS, SPG, FPC, Insula, V1, V2, Cuneus, ITG, MTG, STG, PCC2, PHC1, PHC2, RSC1, RSC2, HIP, HIP1, HIP2, OTC, TP, AG, IPS, A1, A2, PCG, DLPFC, OFC, IPCG, VLPFC, sgACC, IFG, MPFC *Right*: S1, S2, SPG, FPC, Insula, V1, V2, Cuneus, ITG, MTG, STG, PHC1, PHC2, RSC1, RSC2, HIP, HIP1, HIP2, OTC, TP, AG, IPS, A1, A2, PCG, OFC, IPCG, VLPFC, sgACC, IFG, MPFC

hearing thresholds at .125 kHz, .25 kHz, .5 kHz, 1 kHz, 2 kHz, 3 kHz, 4 kHz, 6 kHz and 8 kHz were obtained according to the procedures prescribed by the British Society of Audiology (Audiology, 2008). Further audiometric testing consisted of measuring the pitch and loudness of the perceived tinnitus. This was done by performing a simple analysis of the ear contralateral to the tinnitus ear in patients with unilateral tinnitus and of the ear contralateral to the worst tinnitus ear in patients with bilateral tinnitus. A 1 kHz pure tone was presented to the ear contra lateral to the (worst) tinnitus ear at an intensity that was 10 dB above the patient's hearing threshold in that ear. The pitch of the perceived tinnitus was measured by adjusting the frequency of the 1 kHz tone to match the pitch of the perceived tinnitus. The perceived loudness was matched to the intensity of the tone in a similar way. The tinnitus loudness in dB SL was computed as a difference between the absolute tinnitus loudness in dB HL and the audiometric threshold at the tinnitus frequency (Meeus et al., 2011; Meeus et al., 2009). Table 1 presents an overview of the tinnitus characteristics. This study was approved by the local ethical committee (Antwerp University Hospital) and was in accordance with the declaration of Helsinki. Collection of the data was under approval of IRB UZA OGA85. All patients gave an informed consent.

2.2. Healthy control group

A healthy control group (N = 256; M = 49.514 years; SD = 14.82; 154 males and 102 females) was included in the study. None of these subjects were known to suffer from tinnitus of any kind. Subjects suffering from psychiatric or neurological illness, having a history of psychiatric or drug/alcohol abuse, history of head injury (with loss of consciousness) or seizures, headache, or physical disability were excluded from the study. No hearing assessments were performed on the healthy controls.

2.3. Data collection

Continuous resting state Electroencephalograph (EEG) data was obtained from both the tinnitus and control groups (sampling rate = 500 Hz, band passed 0.15-200 Hz). Subjects in both the

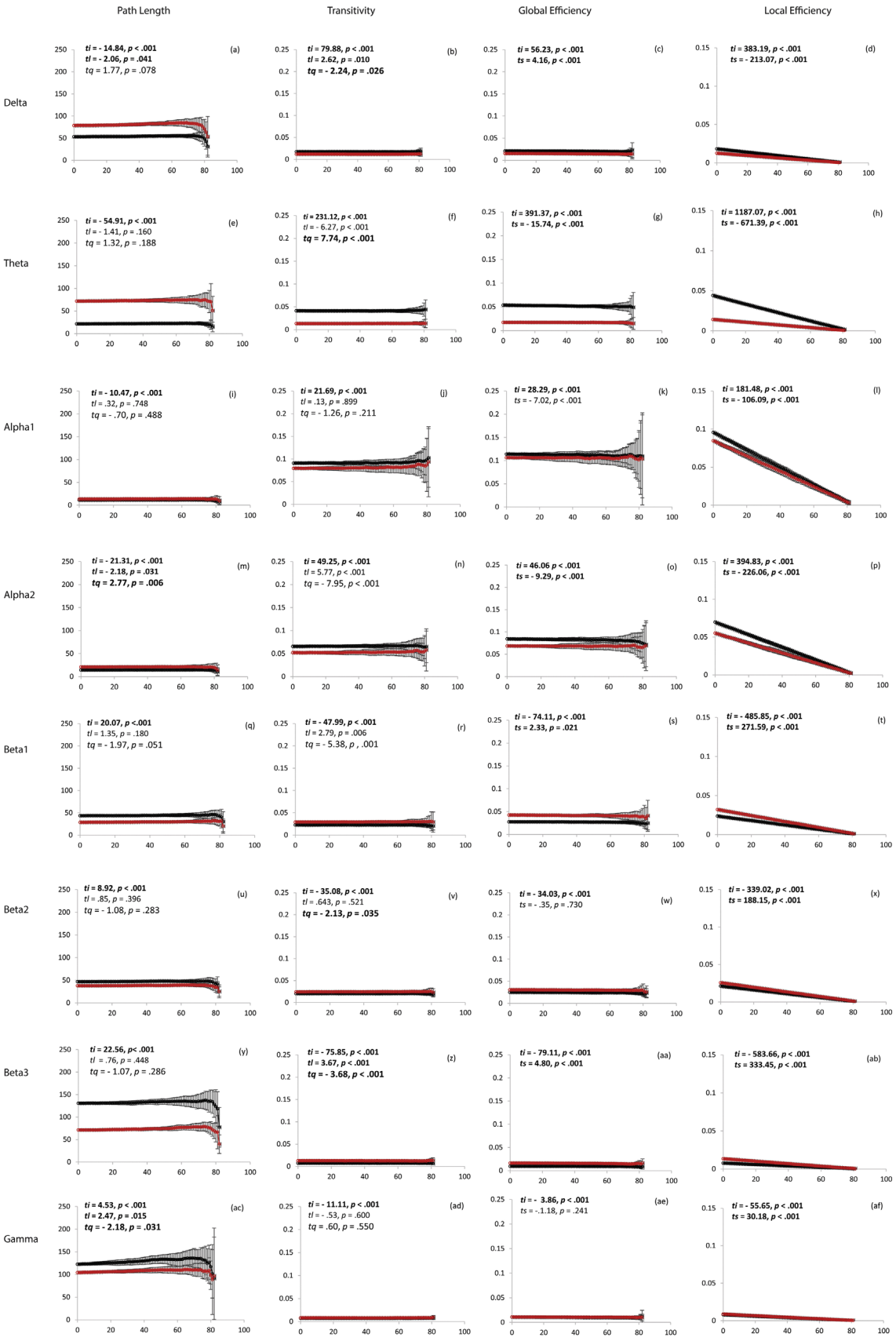

Fig. 2. Change in network connectivity parameters such as path length, transitivity, global and local efficiency as a result of removal of nodes at random in the unthresholded (full) network in the control (black) and tinnitus (red) group respectively in the (a)–(d) delta, (e)–(h) theta, (i)–(l) alpha1, (m)–(p) alpha2, (q)–(t) beta1, (u)–(x) beta2, (y)–(ab) beta3 and (ac)–(af) gamma frequency bands. The *t*-scores depict the two tailed *t*-test for the comparison of the intercept (*ti*), regression coefficients for the linear (*tl*) and quadratic (*tq*) parts of the nonlinear regression. (*ts*) depicts the comparison of the steepness of the slopes of the linear regression between the tinnitus and controls.

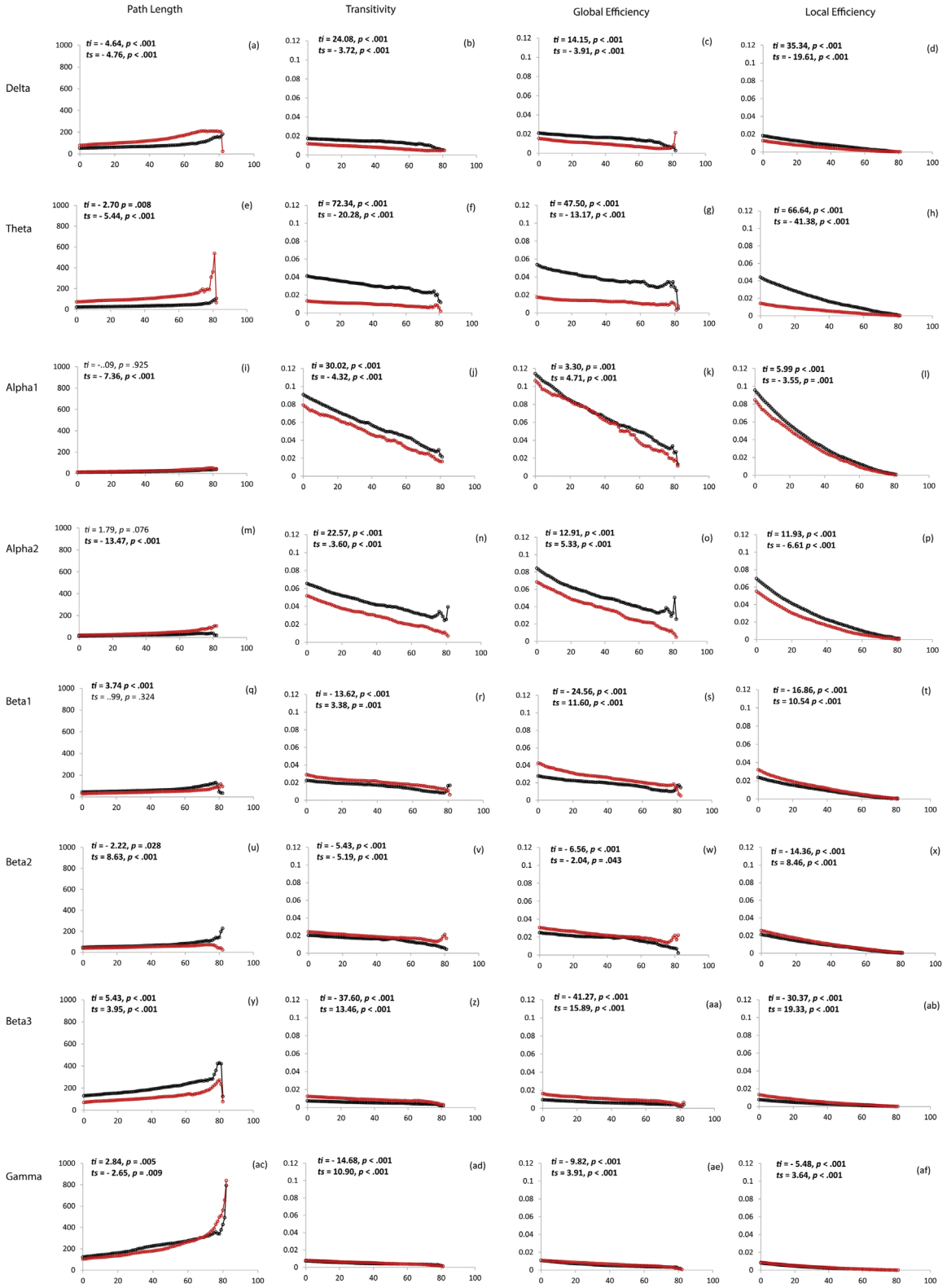

Fig. 3. Change in network connectivity parameters such as path length, transitivity, global and local efficiency as a result of removal of nodes ordered in the decreasing order of betweenness centrality in the unthresholded (full) network in the control (black) and tinnitus (red) group respectively in the (a)–(d) delta, (e)–(h) theta, (i)–(l) alpha1, (m)–(p) alpha2, (q)–(t) beta1, (u)–(x) beta2, (y)–(ab) beta3 and (ac)–(af) gamma frequency bands. The *t*-scores depict the two tailed *t*-test for the comparison of the intercept (*ti*). (*ts*) depicts the comparison of the steepness of the slopes of the linear regression between the tinnitus and controls.

groups were instructed to have their eyes closed condition for five minutes. The participants were made to sit upright on a comfortable chair in a fully lighted room. The EEG data was collected using 19 electrodes (Fp1, Fp2, F7, F3, Fz, F4, F8, T7, C3, Cz, C4, T8, P7, P3, Pz, P4, P8, O1, O2) placed according to the standard 10–20 International placement, sampled using Mitsar-201 amplifiers (NovaTech http://www.novatecheeg.com/) and referenced to digitally linked ears. Impedances on each of the electrodes were

maintained below 5 kΩ. The data was then re-sampled to 128 Hz and band-pass filtering in the range 2–44 Hz as a part of the off-line analysis. The data was then transposed into Eureka! software (Congedo, 2002), where it was carefully plotted and manually inspected for artifacts. Artifacts including eye blinks, eye movements, teeth clenching, body movement, or ECG artifacts were removed from the EEG. This was followed by the computation of average Fourier cross-spectral matrices for 8 frequency bands defined as: delta (2–3.5 Hz), theta (4–7.5 Hz), alpha1 (8–10 Hz), alpha2 (10–12 Hz), beta1 (13–18 Hz), beta2 (18.5–21 Hz), beta3 (21.5–30 Hz) and gamma (30.5–44 Hz). These frequency bands are chosen based on previous tinnitus research (Song et al., 2013a, 2013b; Song et al., 2013a, 2013b; Vanneste and De Ridder, 2011a, 2011b; Vanneste et al., 2010a, 2010b, 2010c; Vanneste et al., 2011a, 2011b; Vanneste et al., 2011a, 2011b).

2.4. Source localization

Intracerebral electrical sources were estimated using the standardized low-resolution brain electromagnetic tomography (sLORETA) sLORETA is useful in computing the neuronal activity in current density (A/m^2) without assuming a predefined number of active sources. A common average reference transformation is performed even before the application of the source-localization algorithm (Pascual-Marqui, 2002). The solution space for the algorithm used in this study along with the lead field matrix are implemented in the LORETA-Key software (freely available at http://www.uzh.ch/keyinst/loreta.htm). This software applies the boundary element method on the MNI-152 (Montreal neurological institute, Canada) Thus, the neocortical volume (including hippocampus and anterior cingulate cortex) in 6239 voxels each having a 5 mm^3 thickness in MNI space is divided and labeled by the sLORETA-key anatomical template based on probabilities returned by the Daemon Atlas.

2.5. Lagged phase coherence

The method we employed here cancels the in-phase correlation between pair-wise sources and does not interfere with their out-of-phase correlations at all frequencies. The residual out-of-phase correlation among sources can be further studied as the coherence between sources in the frequency domain. Such "lagged phase coherence" between sources is interpreted as the amount of cross-talk between the regions contributing to the activity within the sources (Congedo et al., 2010). The cross-talk between the sources can be interpreted as information shared by axonal transmission owing to the coherent, lagged-phase oscillatory property of the sources. The time-series for current density was extracted using sLORETA for all frequency bands defined as mentioned above for all the regions of interest. The regions of interest consist of the 84 Brodmann areas and the values of the lagged phase coherence between each pair-wise combination of Brodmann area signifies the functional connectivity strength between them. Fig. 1 shows locations of the 84 Brodmann areas, and the explanation of the abbreviated region names is given in Table 2.

2.6. Calculation of network connectivity measures

The following measures of network connectivity were calculated using the Brain Connectivity Toolbox (Rubinov and Sporns, 2010a, 2010b) for Matlab™ at the beginning and different stages of the analysis. Further detail will be provided in the course of the methods section.

2.6.1. Characteristic path length

As a first step, the functional connectivity matrix was converted to a connection-length matrix. The shortest distance between pairwise combinations of Brodmann areas was then computed from the connection-length matrix using Dijkstra's algorithm (Dijkstra, 1959). The average shortest path length of the network, termed as the characteristic path length, is the average of the pairwise combinations of shortest path lengths between pairs of Brodmann areas where the distance between two nodes is not equal to infinity (Rubinov and Sporns, 2010a, 2010b). The characteristic path length is a measure of global connectivity.

2.6.2. Transitivity

The transitivity identifies the neighbors of each node and determines the average degree of local connectivity of a node with its neighbors. This was calculated by estimating the number of triangles around a node. Transitivity serves as a measure of local connectivity (Rubinov and Sporns, 2010a, 2010b).

2.6.3. Global efficiency

The global efficiency is the estimate of the efficacy of information transfer between two nodes in the network that are functionally far apart. This is inversely proportional to the characteristic path length of the network. In order to calculate the global efficiency, the shortest distance between pairs of Brodmann areas was first calculated from the functional connectivity matrix as explained above. Next, the characteristic path length of the network was calculated using Dijkstra's algorithm (Dijkstra, 1959). The global efficiency was then estimated as the inverse of the characteristic path length of the network (Rubinov and Sporns, 2010a, 2010b).

2.6.4. Local efficiency

The local efficiency is also a nodal parameter which characterizes the efficiency of information transfer among the neighbors of a particular node. The local efficiency is directly proportional to the clustering coefficient of a node and was calculated from the shortest distance between pairs of Brodmann areas (Rubinov and Sporns, 2010a, 2010b).

2.6.5. Random node attack

Random node attack involves the continuous removal of a random node from the 84 × 84 connectivity matrix and calculating the network connectivity measures mentioned above after the removal of each node. This method is repeated 40 times and the average network connectivity measures along with the standard deviations are calculated over 40 iterations.

2.6.6. Targeted node attack

In this method of successive node removal, the 84 nodes are ordered in descending order of node betweenness centrality. The betweenness centrality reflects the centrality of a node in a network, assuming information transfer follows the shortest path. Therefore, a node with a high betweenness centrality has a large influence on information transmission in the network.

The betweenness centrality of a node is the fraction of the total number of shortest paths that pass through it. It is calculated by examining all the paths passing through a node and summing the number of shortest paths that pass through it, relative to the total number of nodes (Rubinov and Sporns, 2010a, 2010b). The connection weights are converted to connection-length matrices by taking the mathematical inverse of the weighted matrix. The shortest path between any two nodes in the network is then calculated using Dijkstra's algorithm (Dijkstra, 1959). Both the shortest distance between pairs of nodes and the betweenness centrality of each node is determined by appropriate functions from the Brain Connectivity Toolbox (Rubinov and Sporns, 2010a, 2010b).

Thus, the nodes with the highest betweenness centrality are removed first followed by the nodes with lower values of

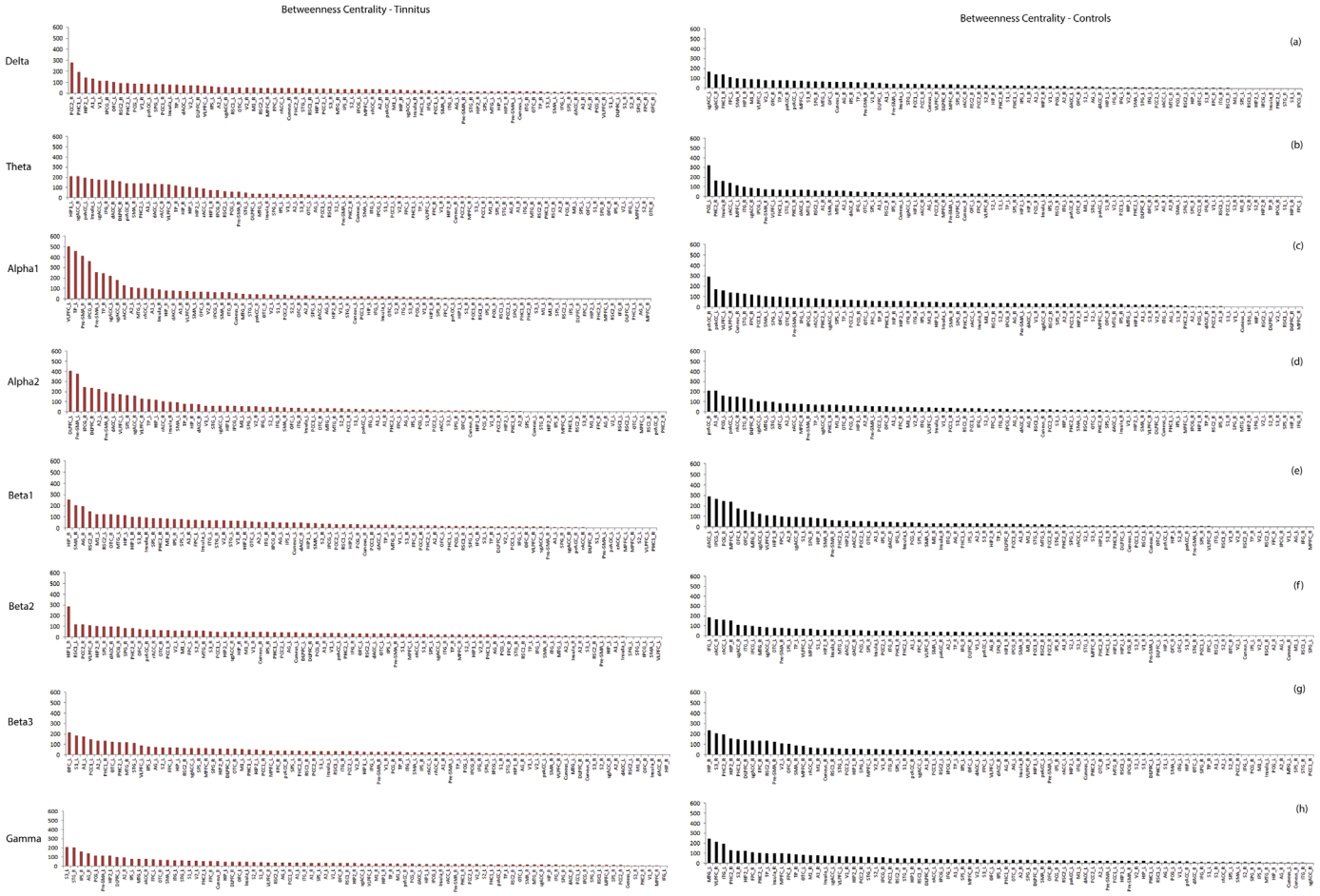

Fig. 4. Hubs ordered in the decreasing order of betweenness centrality in the control (black) and tinnitus group in the (a) delta, (b) theta, (c) alpha1, (d) alpha2, (e) beta1, (f) beta2, (g) beta3, (h) gamma frequency bands in a network thresholded to have equal number of edges in the two groups in the different frequency bands.

betweenness centrality. The four measures of network connectivity are calculated after the removal of each node. No iterations were followed since the order of betweenness centrality will always be the same. This same procedure is followed for the weighted thresholded networks calculated as explained below.

2.6.7. *Calculation of rich club, feeder and local networks (RFL networks)*

The 84 × 84 connectivity matrix is a fully connected matrix where each node is connected to every other node in the network and hence it is difficult to compute the rich club, feeder and the local networks in a fully-connected functional matrix. Thus, a trial and error method was used in order to introduce a threshold in each of the functional matrices for each of the frequency bands such that all the 84 nodes are retained and the number of edges in each of the frequency bands is as equivalent as possible in the two groups. Although maintaining the same number of edges in a group across the different frequency bands was difficult, the number of edges in the tinnitus and the control group in the same frequency band was maintained as close as possible. The thresholds introduced and the number of undirected edges in the two groups across the different frequency bands is given in Table 3. The rich club network is the core structure of a structural or functional connectivity network where each rich club node is connected to every other rich club node (Colizza et al., 2006; M. P. van den Heuvel and Sporns, 2011; Martijn P. van den Heuvel and Sporns, 2013). The feeder network consists of the connections of the nodes in the periphery that directly connect to the rich club node and the local network consist of the connections between nodes in the periphery (Martijn P. van den Heuvel and Sporns, 2013). Sometimes the set of feeder and local nodes might be the same, however the distinguishing factor between the two networks is the connection between the different nodes.

The rich club coefficient is defined as the ratio of the number of edges to the total possible number of edges between the nodes having a degree greater than a certain level k (Colizza et al., 2006). In order to calculate those nodes that satisfy this condition, the rich club coefficient was calculated based on the Brain Connectivity Toolbox (Rubinov and Sporns, 2010a, 2010b) at each of the frequencies for 83 levels, since this is the highest degree attainable for a network with 84 nodes. Rich club coefficients were also generated for 300 random networks derived at each of the frequency bands and an average distribution was drawn over the rich club coefficients of the random networks. The z scores of the rich club coefficients of the subject network were calculated and the first significant level of rich club coefficient was determined as the k-level (rank) above which the rich club nodes were present. The nodes were ordered in the descending order of degree centrality and the nodes with the top 12% of the ranks determined by $.12 * (83\text{-}k)$ were defined to be the rich club nodes. The rich club nodes in the two groups across the different frequency bands are listed in Table 4 and the feeder nodes in the two groups are listed in Table 5.

The non-rich club nodes that directly connected to the rich club nodes were defined to be the feeder nodes and the non-rich club nodes that connected to each other were identified as local nodes. It is important to note that the feeder and local nodes could possibly consist of the same set of nodes.

2.6.8. Node removal in RFL networks

Further analysis is done by successively removing each of the rich club, feeder or local nodes at random and computing the network connectivity measures of the resulting network as mentioned above. This process is repeated 40 times, and the average of the network connectivity measures after the removal of each node is calculated along with the corresponding standard deviations. The average values are then normalized by the number of rich-club, feeder or local nodes in order to perform comparative statistics between the two groups.

2.7. Statistical analysis

The Figs. 3–8 are drawn using the average value of the network parameters generated over 40 iterations and the error bars represent the standard deviation around the mean. Both linear and non-linear regression (quadratic) were applied in a hierarchical way between each of the network connectivity were parameters and the number of nodes removed for each of the groups in the eight frequency bands for both analysis techniques (linear and non-linear). If the proportion of unique variance accounted for by the quadratic model is greater than 10% over and above that contributed by the linear model the quadratic model fit is used else, the linear model fit is used. The difference in the linear and non-linear regression coefficients — the intercept and parameter estimates for the linear and quadratic predictors between the two groups are compared using a two-tailed *t*-test at a significance level of .05 using SPSS.

3. Results

3.1. Random node attack

The quadratic fit for the change in path length and transitivity explains more than 10% of the significant proportion of variance over and above the linear model (Supplementary Table 1). However, this is not the case with global and local efficiency. We observe a significant difference in the y-intercepts of the regression between the two groups for the path length, transitivity, global and local efficiency in the Delta, Theta, Alpha1, Alpha2, Beta1, Beta2, Beta3 and Gamma frequency bands. Significant differences in the linear coefficients of the non-linear regression are observed in the Delta, Alpha2 and Gamma bands for the path length and in the Delta band for transitivity. Significant differences in the quadratic coefficients of the non-linear regression are observed in the Alpha2 and Gamma bands for path length and in the Delta, Theta, Beta2 and Beta3 bands for the transitivity. Significant differences in the linear slope estimates for global efficiency between the two groups is observed in all the frequency bands except in the Alpha1, Beta2 and Gamma bands. The steepness of the slope of local efficiency is however significantly different between the two groups in all the eight frequency bands. The results for the random network attacks are displayed in Fig. 2.

3.2. Targeted attack — full network

We observe that fitting a non-linear regression accounted to less than 10% of unique variance over and above the linear model (Supplementary Table 2). Hence, a linear model was fit for the analysis. We observe a significant difference in the y-intercepts of the regression between the two groups, for all the network connectivity measures in the Delta, Theta, Beta1, Beta2, Beta3 and Gamma frequency bands. The difference in the y-intercepts of the regression between the two groups is significantly different only for the transitivity, global and local efficiency in the Alpha1 and Alpha2 frequency bands. The difference in the steepness of the slope of regression of all the network connectivity measures between the two groups is significant in the Delta, Theta, Alpha1, Alpha2, Beta2, Beta3 and Gamma frequency bands. A significant difference in the steepness of the slope of the transitivity, global and local efficiency is observed in the Beta1 band. The results of the targeted attacks on the full network are displayed in Fig. 3.

3.3. Targeted attack — thresholded networks

The nodes ordered in the decreasing value of betweenness centrality is shown in Fig. 4. In contrast to the model fit of the Targeted Attack on the full network, the Targeted Attack on the thresholded network follows a non-linear trend for the path length and transitivity and a linear trend for the global and local efficiency (Supplementary Table 3). We observe a significant difference in the y-intercepts of the regression between the two groups, for all the network connectivity measures in the Theta, Beta1, Beta2 and Beta3 frequency bands. The difference in the y-intercepts of the regression between the two groups is significantly different only for the path length, global and local efficiency in the Delta band, local efficiency in the Alpha1 and Alpha2 bands, transitivity, local and global efficiency in the Gamma frequency band. The difference in the linear coefficients of the non-linear regression for the pathlength and transitivity is significant in all the frequency bands except Beta2. The difference in the quadratic slope is significant for both path length and transitivity in all the bands, except for the path length in the Beta 2 band. The steepness of the slope of the linear regression for the global and local efficiency for all the network connectivity measures between the two groups is significant in all the frequency bands except for global efficiency in the Delta, Alpha1 and Beta2 bands. The results for the Targeted Attack in the thresholded network are displayed in Fig. 5.

3.4. Rich club node removal

Comparing the proportion of variance accounted for by the quadratic and linear regression models, we observe that the quadratic model did not add more than 10% of unique variance over above the linear model (Supplementary Table 4). Hence, we fit a linear model to the analysis. A significant difference in the y-intercepts of the regression of all the network connectivity measures is found between the tinnitus and control groups in the Delta, Theta, Alpha1, Alpha2, Beta1, Beta2 and Gamma frequency bands. In the Beta3 frequency band, we observe that the difference in y-intercepts of the regression of only the path length is significantly different between the two groups and that of the transitivity, global and local efficiency are not statistically significant. The difference in the steepness of the slopes of the regression of all the network connectivity measures between the two groups are statistically significant across all the frequency bands. The results for the rich club node removal analysis are displayed in Fig. 6.

3.5. Feeder network node removal

Comparing the linear and non-linear model fit, we observe that the quadratic regression adds more than 10% of unique variance to the linear model over and above the proportion of variance explained by it (Supplementary Table 5). This was observed only for the path length and transitivity and hence we fit a quadratic model to the path length and transitivity whereas fit a linear model to the global and local efficiency. We observe a significant difference in the y-intercepts of the regression of path length, transitivity, global and local efficiency between the tinnitus and control groups in all the frequency bands except for global efficiency in Alpha2 and

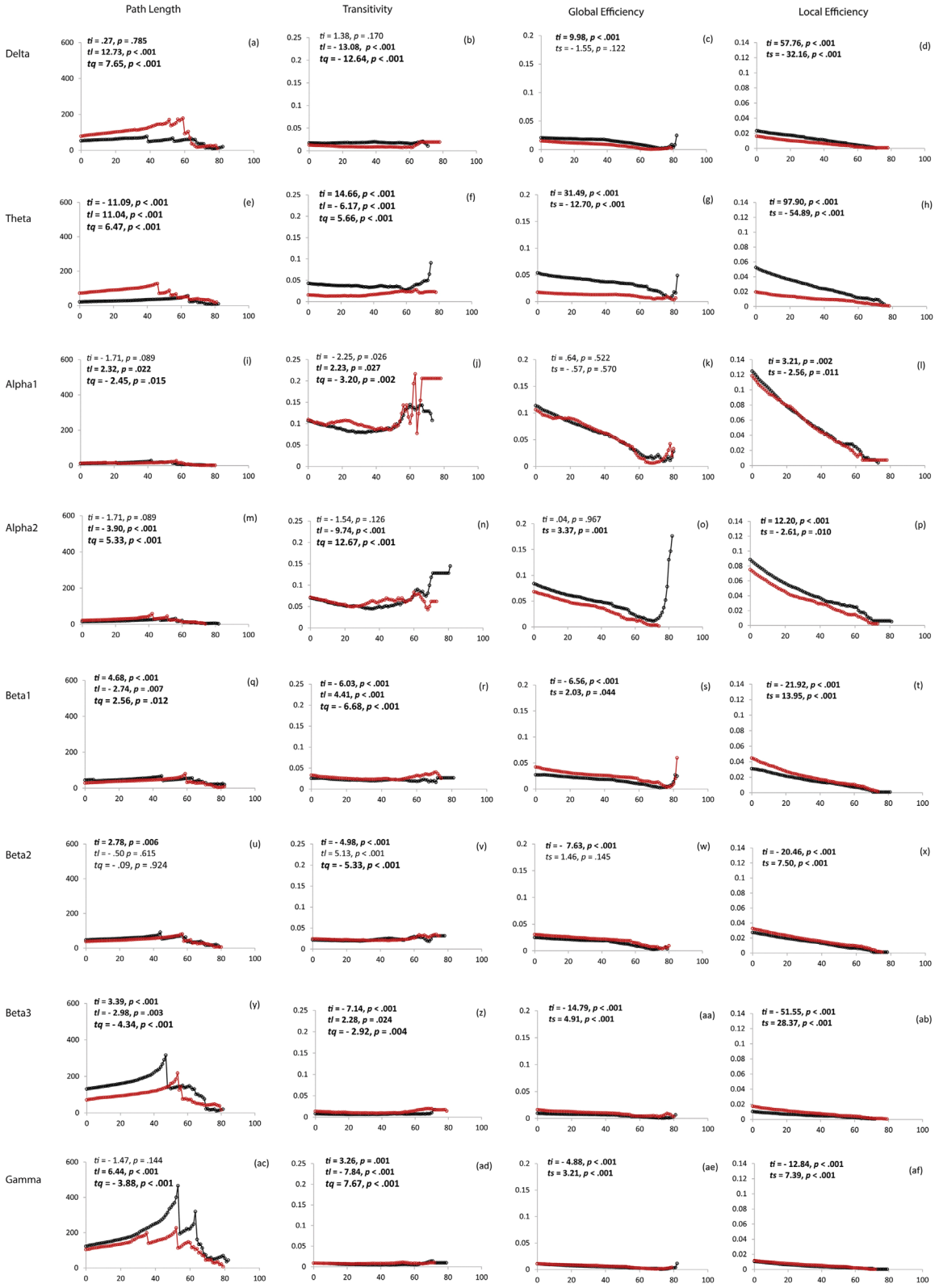

Fig. 5. Change in network connectivity parameters such as path length, transitivity, global and local efficiency as a result of removal of nodes ordered in the decreasing order of betweenness centrality in the thresholded network with equal number of edges in the control (black) and tinnitus (red) group respectively in the (a)–(d) delta, (e)–(h) theta, (i)–(l) alpha1, (m)–(p) alpha2, (q)–(t) beta1, (u)–(x) beta2, (y)–(ab) beta3 and (ac)–(af) gamma frequency bands. The *t*-scores depict the two tailed *t*-test for the comparison of the intercept (*ti*), regression coefficients for the linear (*tl*) and quadratic (*tq*) parts of the nonlinear regression. (*ts*) depicts the comparison of the steepness of the slopes of the linear regression between the tinnitus and controls.

Transitivity in the Gamma band. The difference in linear slope coefficient of the non-linear regression between the two groups is significant for the path length in the Delta, Theta, Beta3 and Gamma bands and for the transitivity in all the frequency bands except the Delta band. The difference in the coefficient of the quadratic relationship is significant for both the path length and

transitivity in the Delta, Theta, Alpha2, Beta3 and Gamma bands, however for transitivity it is significant only for Beta1 and path length in Beta2 (and gamma). The difference in the steepness of the linear regression for both the global and local efficiency are significant in all the frequency bands except for global efficiency in the Gamma band. The results of the feeder network node removal analysis are displayed in Fig. 7.

3.6. Local network node removal

Similar to the attack on the feeder network, the attack on the local network follows a nonlinear trend for the path length and transitivity and a linear trend for the global and local efficiency (Supplementary Table 6). The difference in the y-intercepts of the regression is significant for all the measures of network connectivity across all frequency bands with the exception of global efficiency in the Alpha2 band and transitivity in the Theta band. The difference in the linear slopes of the nonlinear regression is significant for both the path length and transitivity in the Delta, Theta, Beta1, Beta3 and Gamma bands between the two groups. The difference in the linear slope is significant only for the transitivity in the Alpha2 and Beta2 bands. The difference in slope of the quadratic portion of the non-linear regression is significant for both path length and transitivity in all the frequency bands with the exception of path length in the Beta2 band. The difference in the steepness of the slope of the linear regression for the global and local efficiency is significant for the both measures in all the frequency bands with the exception of global efficiency in the Alpha2 and Gamma bands. The results for the local network node removal analysis are displayed in Fig. 8.

4. Discussion

The current study models the dynamics of functional networks in tinnitus when a virtual lesion is introduced to nodes at random in contrast to specific groups of nodes, i.e. to a targeted attack (Reka Albert et al., 2000). These specific nodes are selected on the basis of either betweenness centrality or the participation of the node in the rich club, feeder or local network. In addition, the study also aims to provide evidence for a multimodal organization of functional networks in the brain and further discusses disorder specific changes to this organization in tinnitus.

Comparing the network attributes in the two groups, we observe that the tinnitus network is fundamentally different from the control network. Comparing the intercepts of the network properties in tinnitus and control group, i.e. the network properties when no nodes are removed, the tinnitus group shows a decrease in long distance connectivity, by virtue of an increase in path length and decrease in global efficiency for the lower frequency bands and increase in short distance connectivity characterized by an increase in these measures in the higher frequency bands. This comparison of the intercepts is consistent with our previous study (Mohan et al., 2016) on the same dataset where we showed a similar pattern of results by comparing network parameters of the tinnitus group with the control group. This indicates an aberration from the usually observed “small-world” topology of the normal brain connectome, characterized by a clique community structure that is integrated by a small number of cross-modal connections (Bassett Danielle Smith and Bullmore, 2006; Mohan et al., 2016; Sporns O. and Zwi, 2004; Watts, Duncan J. 1999; Watts D. J. and Strogatz, 1998). The decrease in cluster coefficient and increase in path length suggests a more diffuse organization within the communities in lower frequency bands. In contrast, an increase in cluster coefficient and path length in the higher frequency bands suggest the presence of tighter knit communities that are more randomly connected. Such disorder specific changes in network topology have been reported in other disorders such as Alzheimer's (de Haan et al., 2009; Stam et al., 2009; Stam et al., 2007), Parkinson's (Olde Dubbelink et al., 2014; Stam, 2010), schizophrenia (D. S. Bassett et al., 2008; Stam, 2010), epilepsy (Stam, 2014; Vecchio et al., 2015), traumatic brain injury (Cao and Slobounov, 2010; Pandit et al., 2013) and is described as changes in efficiency of local and global processing of information.

Although tinnitus is identified by an aberrant topology, the scale-free aspect (Sporns et al., 2004; Strogatz, 2001; Wuchty, 2001) of the network still seems to be intact. We observe that only a small number of nodes are characterized by a high betweenness centrality value indicating that only a small portion of the nodes contribute to integrating information from different communities. In our data, this is further confirmed by the resilience of the network to the removal of nodes at random and a rapid degradation of network properties when the nodes with maximum betweenness centrality are removed first. It is important to note here that although a non-linear fit was used to model the random attack and a linear fit was used to model the targeted attack analyses, the visual inspection of the scatter plots show that the random attack turns rapidly non-linear when most of the nodes are removed from the network. Until that point, the network does not show a dynamic trend. In contrast, the targeted attack on the betweenness centrality shows a steep linear change which also turns non-linear when most of the nodes are removed from the network. The non-linearity did not statistically add any more unique variance to the linear model and hence was disregarded. Taking a closer look at the specific parameters, we observe that there is a steep decline in the global efficiency (long distance communication) and transitivity (short distance communication) when nodes with maximum betweenness centrality are targeted in comparison with removing nodes at random. These results are in agreement with the results of Alstott et al., (Alstott et al., 2009) where they show a rapid decline in the global efficiency of the network on removing nodes with maximum betweenness centrality.

Brain networks are also known to have a core-periphery structure (Danielle S Bassett and Lynall, 2013). Unlike the conventional core-periphery structure which has a densely connected core and a sparsely connected periphery (Borgatti and Everett, 2000; Holme, 2005; Rombach et al., 2014; Zhang et al., 2015), the core structure in the brain is found to be an integration of the communities by means of a tight-knit rich club network (Senden et al., 2014; Olaf Sporns, 2013; M. P. van den Heuvel and Sporns, 2011). The rich-club is a group of highly interconnected nodes (Colizza et al., 2006; McAuley et al., 2007; M. P. van den Heuvel and Sporns, 2011) which forms a functional substrate for increased global access of functional regions (Collin et al., 2014) and increased global efficiency of information transfer (Bullmore and Sporns, 2012; Senden et al., 2014). Indeed, we observe that the removal of nodes from the rich-club network has a similar effect on the network dynamics as the removal of nodes at random. This can be seen in the functional form of the change in different network parameters specifically in the path length, transitivity and global efficiency in the random node removal and the rich club node removal indicating a preservation of network properties. This pattern is identified in both groups and is indicative of the relative resilience of the rich-club network as reported in previous research (Achard et al., 2006). This robustness of the rich-club network is critical in providing a physiological substrate for segregated and distributed information processing (S. Achard et al., 2006; Alstott et al., 2009). Thus the resilience and robustness of the rich club network further bolsters the idea of the importance of the rich-club in functionally integrating the segregated peripheral communities (Olaf Sporns, 2013) and increasing the efficiency of the network (Bullmore and Sporns, 2012; Collin et al.,

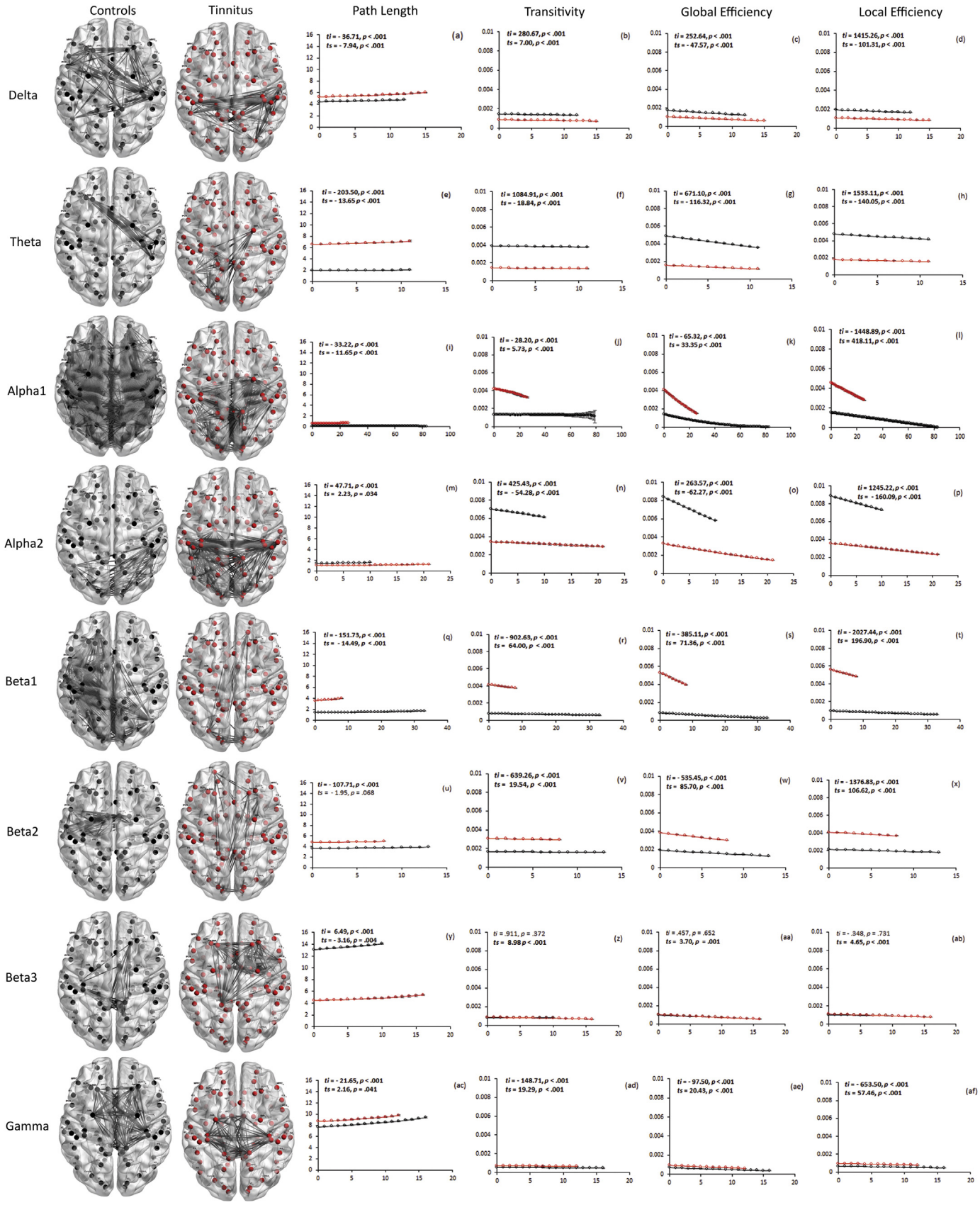

Fig. 6. The brain images show the rich club network in the control (black) and tinnitus (red) group in the delta, theta, alpha1, alpha2, beta1, beta2, beta3 and gamma frequency bands. The graphs show the change in the network properties such as the path length, transitivity, global and local efficiency as a result of the removal of the nodes of the rich club network in the (a)–(d) delta, (e)–(h) theta, (i)–(l) alpha1, (m)–(p) alpha2, (q)–(t) beta1, (u)–(x) beta2, (y)–(ab) beta3 and (ac)–(af) gamma frequency bands. The *t*-scores depict the two tailed *t*-test for the comparison of the intercept (*ti*). (*ts*) depicts the comparison of the steepness of the slopes of the linear regression between the tinnitus and controls.

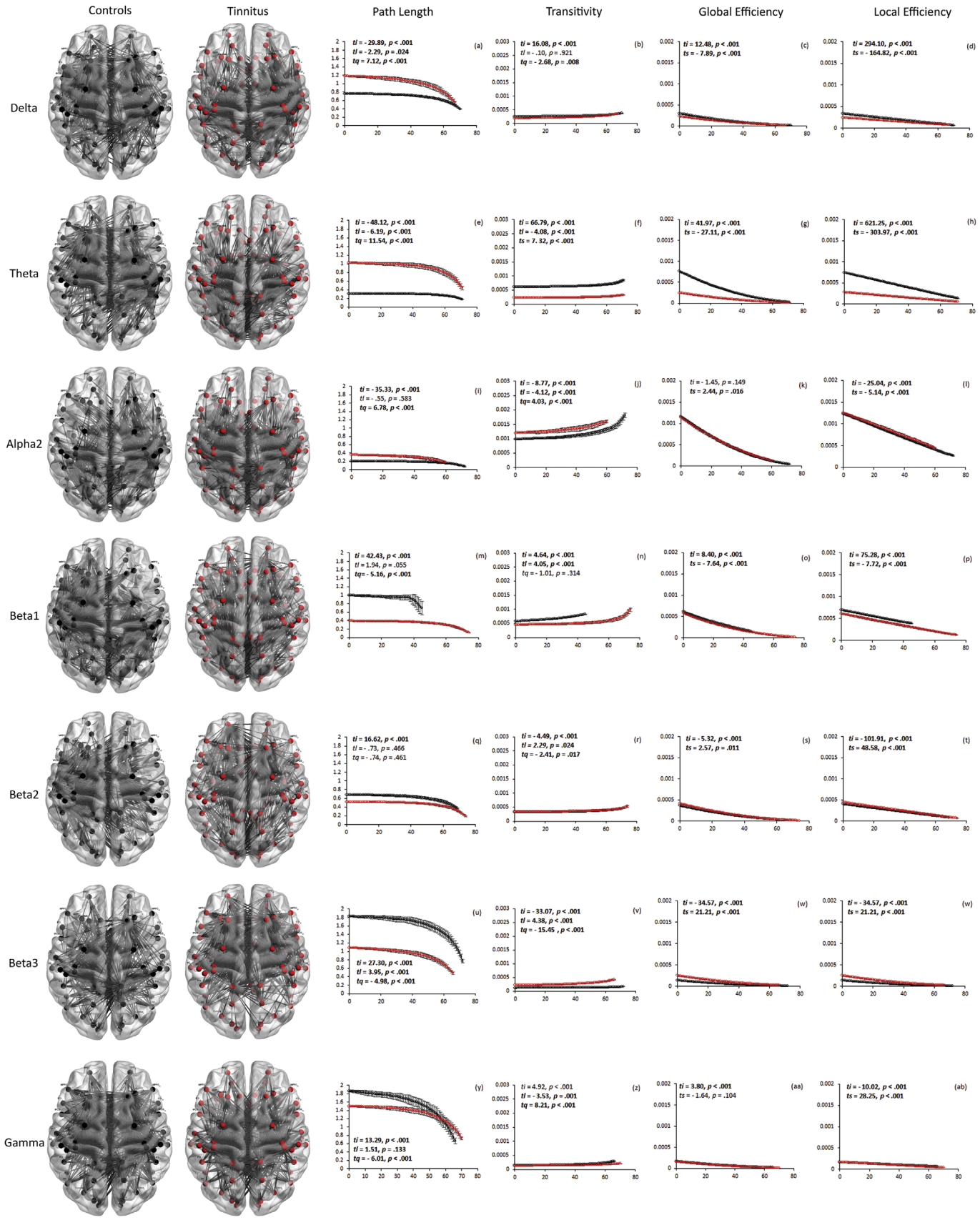

Fig. 7. The brain images show the feeder network in the control (black) and tinnitus (red) group in the delta, theta, alpha2, beta1, beta2, beta3 and gamma frequency bands. The graphs show the change in the network properties such as the path length, transitivity, global and local efficiency as a result of the removal of the nodes of the feeder network in the (a)–(d) delta, (e)–(h) theta, (i)–(l) alpha2, (m)–(p) beta1, (q)–(t) beta2, (u)–(x) beta3 and (y)–(ab) gamma frequency bands. The *t*-scores depict the two tailed *t*-test for the comparison of the intercept (*ti*), regression coefficients for the linear (*tl*) and quadratic (*tq*) parts of the nonlinear regression. (*ts*) depicts the comparison of the steepness of the slopes of the linear regression between the tinnitus and controls.

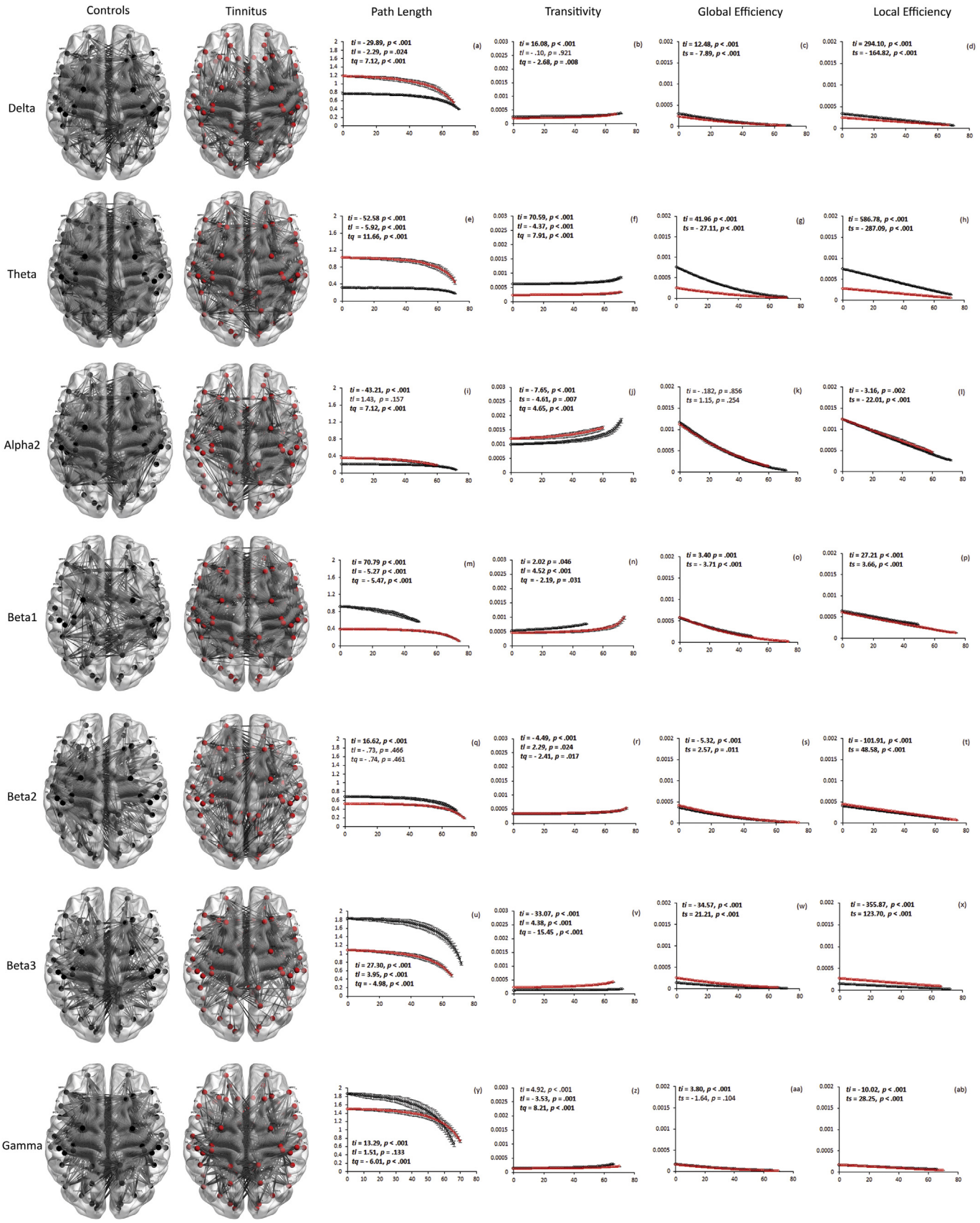

Fig. 8. The brain images show the local network in the control (black) and tinnitus (red) group in the delta, theta, alpha2, beta1, beta2, beta3 and gamma frequency bands. The graphs show the change in the network properties such as the path length, transitivity, global and local efficiency as a result of the removal of the nodes of the local network in the (a)–(d) delta, (e)–(h) theta, (i)–(l) alpha2, (m)–(p) beta1, (q)–(t) beta2, (u)–(x) beta3 and (y)–(ab) gamma frequency bands. The *t*-scores depict the two tailed *t*-test for the comparison of the intercept (*ti*), regression coefficients for the linear (*tl*) and quadratic (*tq*) parts of the nonlinear regression. (*ts*) depicts the comparison of the steepness of the slopes of the linear regression between the tinnitus and controls.

2014). However, this is a downside in the tinnitus network. Since the rich-club network in the different frequency bands contain some of the important regions shown to encode either the loudness, distress, core or conscious percept, its resilience is undesirable while making an attempt to modify the tinnitus percept.

In contrast, a common pattern in the dynamicity of network parameters was observed on comparing the effect of removing nodes based on betweenness centrality (in the full and thresholded network) and the feeder network. In the thresholded network, we observe that there is a non-linear decline in the path length and transitivity when nodes of high-betweenness centrality are targeted, which is consistent with changes in the path length and transitivity as a result of an attack on the feeder network. Although the targeted attack on the full network follows a linear decline, the difference in the functional form between the targeted attack on the full network and the attack on the feeder network may be attributed to the thresholding itself. A significant non-linear change in the transitivity and average path length and a steep decline in the local and global efficiency of the network on attacking the feeder network was detected in both the groups reflecting respective changes in short and long distance connectivity. This alludes to the idea that the hubs connecting different communities (Albert et al., 2004; Han et al., 2004) together are possibly located in the feeder network. Secondly, we observe that in both groups, nodes with the highest betweenness centrality, for the most part, are not part of the rich club but are part of feeder network. Since the feeder nodes connect directly to the rich club (Martijn P. van den Heuvel and Sporns, 2013) and are also central to the network structure, they present a tendency to drive the functional dynamics of the network by integrating the different modules. Thus, virtual focal lesions in the feeder nodes create a diffuse effect on inter-regional synchronization dynamics that extend well beyond the affected site (Honey and Sporns, 2008). To tinnitus, this would mean that the most vulnerable sites in the network lie in the periphery and are those that connect the different communities in the periphery to the core rich club. Thus, removing feeder nodes, in other words, disconnecting the communities from the core seems to be a very effective way of modifying the tinnitus network. Targeting peripheral nodes as a prospective treatment method has been presented in protein–protein interaction networks (Barabási, 2007; Barabasi et al., 2011). It was shown that the disease-encoding proteins were found in the periphery and not in the core, since the core network was important in the performing life-sustaining activities (Goh et al., 2007).

Looking closely at the structures involved in the specific networks, we observe that the rich club-networks identified in the tinnitus and control network are strikingly different in all the frequency bands. In the control network we find that the nodes of the auditory resting state network (Husain and Schmidt, 2014; Mantini et al., 2007) can be identified in the rich-club of the beta frequency band, particularly in the beta1 frequency band. The primary sensory cortices in the visual and somatosensory resting state networks and the nodes of the default mode network (Mantini et al., 2007) seem to be distributed over the rich-club networks in all the frequency bands. However the nodes in the rich-club of the tinnitus network in specific frequency bands correspond to specific sub-networks identified in previous tinnitus literature. In the current study the nodes of the tinnitus core (inferior parietal area, parahippocampal area and auditory cortices) (De Ridder et al., 2014a, 2014b) and loudness networks (auditory cortices and parahippocampal area) (De Ridder et al., 2013; Husain and Schmidt, 2014) are found in the delta, theta and alpha frequency bands. The nodes in the rich club of the beta band, specifically the beta3 band seem to house the nodes such as the precuneus, insula, pregenual, subgenual and dorsal anterior cingulate cortex that are generally observed in the network encoding tinnitus distress (Husain and Schmidt, 2014; Mayberg et al., 2005; Vanneste et al., 2010a, 2010b, 2010c; Weisz et al., 2005). It is also proposed that the unified tinnitus percept produced by these interacting-subnetworks is brought to consciousness (De Ridder et al., 2014a, 2014b; Schlee et al., 2009) by the global neuronal workspace encoded by the gamma band (Dehaene et al., 2006). The nodes in the rich club of the gamma band, from the current study are in agreement with previous research that have identified the regions such as inferior and superior parietal sulci that maybe part of this workspace (Schlee et al., 2009).

From the current analyses we understand that functional networks in the brain consist of individual and separable functional modules which is built as a combination of both a community structure as well a core-peripheral structure (Olaf Sporns, 2013), unique to each oscillatory band. Each of these modules consists of a resilient and densely connected core called the rich-club network which is robust, even to selectively targeted lesions. The rich-club network is coupled with the peripheral network, which is organized in communities, by means of feeder nodes which are functionally central to the module. Owing to the centrality of feeder nodes, damage/intervention to these sites results in dynamic changes in the connectivity profile of the module resulting in the disconnection of the communities from the core. Further, it has been shown that there exists an aberrant cross-frequency coupling in tinnitus between different regions in the brain (Adamchic et al., 2014; De Ridder et al., 2014a, 2014b). This nesting of high-frequency signals on a low-frequency carrier wave aids in the transmission of high frequency information over long distances (Canolty and Knight, 2010). This is one of the hypotheses behind the global broadcast of the conscious percept in the gamma band (De Ridder et al., 2014a, 2014b). Due to this possibility of a cross-frequency coupling, which is not explored in the current study, we also propose that the functional modules in each of the frequency bands overlap with each other producing a complex network structure. This may be one of the reasons as to why treatment for this disorder seems to work only for a part of the population and not the rest (Dirk De Ridder et al., 2013; De Ridder et al., 2012; Engelhardt et al., 2014; Vanneste and De Ridder, 2011a, 2011b; Vanneste et al., 2010a, 2010b, 2010c; Vanneste et al., 2010a, 2010b, 2010c).

One of the main drawbacks of the study is that the control group is not matched for hearing loss with the tinnitus group. Since hearing loss is one of the major comorbidities of tinnitus (Norena et al., 2002) the results of the current study should be confirmed by further research that controls for hearing loss. Second, the procedure involves an indirect way of localizing the sources. Although EEG has a high temporal resolution and source localization techniques have improved, it is still important to understand that these results have to be confirmed by higher (spatial) resolution techniques such as fMRI. Furthermore, the current study analyzes the effect of the removal of complete nodes and its associated connections which is analogous to removing whole brain regions from a surgical perspective. This calls for research investigating the dynamics of a network based on changing specific parameters in weighted networks such as connection weights, number of edges etc. Moreover, removal of just nodes does not effectively contrast the effect of attacking the feeder versus local networks, since there is a large overlap in the nodes of the two networks. The current study is a first step in understanding the organization and dynamics of normal and disorder specific functional networks under the effect of virtual focal lesions.

In conclusion, brain networks are organized in a multimodular network of overlapping modules which consist of a functionally resilient core and a community-abundant periphery. The feeders are functionally central to the network topology and integrates the different modules. Considering tinnitus, the networks encoding tinnitus are distributed in the rich club of different frequency bands and seem to be functionally integrated to the peripheral modules by the feeder nodes. Thus the modification of the tinnitus

network is proposed to be most effective by targeting the feeder nodes thereby disconnecting the modules from the core. Future research in this domain using different tools to analyze functional networks may provide a clearer view of the organization of the tinnitus network. Nevertheless, the current analysis presents a testable hypothesis and a promising future for modifying pathological networks based on network connectivity analysis.

Appendix A. Supplementary material

Supplementary data to this article can be found online at http://dx.doi.org/10.1016/j.neuroimage.2016.04.033.

References

Achard, S., Bullmore, E., 2007. Efficiency and cost of economical brain functional networks. PLoS Comput. Biol. 3 (2), e17. http://dx.doi.org/10.1371/journal.pcbi.0030017.

Achard, S., Salvador, R., Whitcher, B., Suckling, J., Bullmore, E., 2006. A resilient, low-frequency, small-world human brain functional network with highly connected association cortical hubs. J. Neurosci. 26 (1), 63–72 (doi:26/1/63).

Adamchic, I., Langguth, B., Hauptmann, C., Tass, P.A., 2014. Abnormal cross-frequency coupling in the tinnitus network. Front. Neurosci. 8, 284. http://dx.doi.org/10.3389/fnins.2014.00284.

Albert, R., Jeong, H., Barabasi, A.-L., 2000. Error and attack tolerance of complex networks. Nature 406 (6794), 378–382.

Albert, R., Albert, I., Nakarado, G.L., 2004. Structural vulnerability of the north American power grid. Phys. Rev. E 69 (2), 025103.

Alstott, J., Breakspear, M., Hagmann, P., Cammoun, L., Sporns, O., 2009. Modeling the impact of lesions in the human brain. PLoS Comput. Biol. 5 (6), e1000408 http://dx.doi.org/10.1371/journal.pcbi.1000408.

Audiology, B.S.o., 2008. Recommended Procedure: Pure Tone Air and Bone Conduction Threshold Audiometry with and without Masking and Determination of Uncomfortable Loudness Levels.

Barabási, A.-L., 2007. Network medicine — from obesity to the "Diseasome". N. Engl. J. Med. 357 (4), 404–407. http://dx.doi.org/10.1056/NEJMe078114.

Barabasi, A.-L., Gulbahce, N., Loscalzo, J., 2011. Network medicine: a network-based approach to human disease. Nat. Rev. Genet. 12 (1), 56–68.

Bassett, D.S., Bullmore, E., 2006. Small-world brain networks. Neuroscientist 12 (6), 512–523. http://dx.doi.org/10.1177/1073858406293182.

Bassett, D.S., Lynall, M.-E., 2013. Network methods to characterize brain structure and function, Cognitive Neurosciences. The Biology of the Mind.

Bassett, D.S., Bullmore, E., Verchinski, B.A., Mattay, V.S., Weinberger, D.R., Meyer-Lindenberg, A., 2008. Hierarchical organization of human cortical networks in health and schizophrenia. J. Neurosci. 28 (37), 9239–9248 (doi:28/37/9239).

Borgatti, S.P., Everett, M.G., 2000. Models of core/periphery structures. Soc. Networks 21 (4), 375–395.

Bullmore, E., Sporns, O., 2012. The economy of brain network organization. Nat. Rev. Neurosci. 13 (5), 336–349. http://dx.doi.org/10.1038/nrn3214.

Canolty, R.T., Knight, R.T., 2010. The functional role of cross-frequency coupling. Trends Cogn. Sci. 14 (11), 506–515. http://dx.doi.org/10.1016/j.tics.2010.09.001.

Cao, C., Slobounov, S., 2010. Alteration of cortical functional connectivity as a result of traumatic brain injury revealed by graph theory, ICA, and sLORETA analyses of EEG signals. IEEE Trans. Neural Syst. Rehabil. Eng. 18 (1), 11–19. http://dx.doi.org/10.1109/TNSRE.2009.2027704.

Colizza, V., Flammini, A., Serrano, M.A., Vespignani, A., 2006. Detecting rich-club ordering in complex networks. Nat. Phys. 2 (2), 110–115.

Collin, G., Sporns, O., Mandl, R.C.W., van den Heuvel, M.P., 2014. Structural and functional aspects relating to cost and benefit of Rich Club Organization in the Human Cerebral Cortex. Cereb. Cortex (New York, NY) 24 (9), 2258–2267. http://dx.doi.org/10.1093/cercor/bht064.

Congedo, M., 2002. EureKa! (Version 3.0) [Computer Software]. NovaTech EEG Inc., Knoxville, TN (Freeware available at www.NovaTechEEG).

Congedo, M., John, R.E., De Ridder, D., Prichep, L., Isenhart, R., 2010. On the "dependence" of "independent" group EEG sources; an EEG study on two large databases. Brain Topogr. 23 (2), 134–138. http://dx.doi.org/10.1007/s10548-009-0113-6.

de Haan, W., Pijnenburg, Y.A.L., Strijers, R.L.M., van der Made, Y., van der Flier, W.M., Scheltens, P., Stam, C.J., 2009. Functional neural network analysis in frontotemporal dementia and Alzheimer's disease using EEG and graph theory. BMC Neurosci. 10, 101. http://dx.doi.org/10.1186/1471-2202-10-101.

De Ridder, D., Vanneste, S., Menovsky, T., Langguth, B., 2012. Surgical brain modulation for tinnitus: the past, present and future. J. Neurosurg. Sci. 56 (4), 323–340.

De Ridder, D., Song, J.-J., Vanneste, S., 2013. Frontal cortex TMS for tinnitus. Brain Stimul. 6 (3), 355–362.

De Ridder, D., Vanneste, S., Freeman, W., 2014a. The Bayesian brain: phantom percepts resolve sensory uncertainty. Neurosci. Biobehav. Rev. 44 (0), 4–15.

De Ridder, D., Vanneste, S., Weisz, N., Londero, A., Schlee, W., Elgoyhen, A.B., Langguth, B., 2014b. An integrative model of auditory phantom perception: tinnitus as a unified percept of interacting separable subnetworks. Neurosci. Biobehav. Rev. 44, 16–32. http://dx.doi.org/10.1016/j.neubiorev.2013.03.021.

Dehaene, S., Changeux, J.-P., Naccache, L., Sackur, J., Sergent, C., 2006. Conscious, preconscious, and subliminal processing: a testable taxonomy. Trends Cogn. Sci. 10 (5), 204–211.

Dijkstra, E.W., 1959. A note on two problems in connexion with graphs. Numer. Math. 1 (1), 269–271. http://dx.doi.org/10.1007/BF01386390.

Doyle, J.C., Alderson, D.L., Li, L., Low, S., Roughan, M., Shalunov, S., … Willinger, W., 2005. The "robust yet fragile" nature of the internet. Proc. Natl. Acad. Sci. U. S. A. 102 (41), 14497–14502. http://dx.doi.org/10.1073/pnas.0501426102.

Engelhardt, J., Dauman, R., Arné, P., Allard, M., Dauman, N., Branchard, O., … Cuny, E., 2014. Effect of chronic cortical stimulation on chronic severe tinnitus: a prospective randomized double-blind cross-over trial and long-term follow up. Brain Stimul. 7 (5), 694–700.

Flake, G.W., Lawrence, S., Giles, C.L., Coetzee, F.M., 2002. Self-organization and identification of web communities. Computer 35 (3), 66–71. http://dx.doi.org/10.1109/2.989932.

Fortunato, S., 2010. Community detection in graphs. Phys. Rep. 486 (3–5), 75–174.

Goh, K.-I., Cusick, M.E., Valle, D., Childs, B., Vidal, M., Barabási, A.-L., 2007. The human disease network. Proc. Natl. Acad. Sci. 104 (21), 8685–8690.

Han, J.-D.J., Bertin, N., Hao, T., Goldberg, D.S., Berriz, G.F., Zhang, L.V., … Vidal, M., 2004. Evidence for dynamically organized modularity in the yeast protein–protein interaction network. Nature 430 (6995), 88–93.

Holme, P., 2005. Core-periphery organization of complex networks. Phys. Rev. E 72 (4), 046111.

Honey, C.J., Sporns, O., 2008. Dynamical consequences of lesions in cortical networks. Hum. Brain Mapp. 29 (7), 802–809. http://dx.doi.org/10.1002/hbm.20579.

Husain, F.T., Schmidt, S.A., 2014. Using resting state functional connectivity to unravel networks of tinnitus. Hear. Res. 307 (0), 153–162.

Jeong, H., Mason, S.P., Barabasi, A.L., Oltvai, Z.N., 2001. Lethality and centrality in protein networks. Nature 411 (6833), 41–42.

Langguth, B., Kreuzer, P.M., Kleinjung, T., De Ridder, D., 2013. Tinnitus: causes and clinical management. Lancet Neurol. 12 (9), 920–930. http://dx.doi.org/10.1016/S1474-4422(13)70160-1.

Mantini, D., Perrucci, M.G., Del Gratta, C., Romani, G.L., Corbetta, M., 2007. Electrophysiological signatures of resting state networks in the human brain. Proc. Natl. Acad. Sci. U. S. A. 104 (32), 13170–13175.

Mayberg, H.S., Lozano, A.M., Voon, V., McNeely, H.E., Seminowicz, D., Hamani, C., … Kennedy, S.H., 2005. Deep brain stimulation for treatment-resistant depression. Neuron 45 (5), 651–660.

McAuley, J.J., da Fontoura Costa, L., Caetano, T.S., 2007. Rich-club phenomenon across complex network hierarchies. Appl. Phys. Lett. 91 (8), 084103.

Meeus, O., Heyndrickx, K., Lambrechts, P., De Ridder, D., Van de Heyning, P., 2009. Phase-shift treatment for tinnitus of cochlear origin. Eur. Arch. Otorhinolaryngol. http://dxdoi.org/10.1007/s00405-009-1145-y

Meeus, O., De Ridder, D., Van de Heyning, P., 2011. Administration of the combination Clonazepam–Deanxit as treatment for tinnitus. Otol. Neurotol. http://dxdoi.org/10.1097/MAO.0b013e31820e737c

Mohan, A., De Ridder, D., Vanneste, S., 2016. Graph theoretical analysis of brain connectivity in phantom sound perception. Sci. Report. 6, 19683. http://dx.doi.org/10.1038/srep19683.

Norena, A., Micheyl, C., Chery-Croze, S., Collet, L., 2002. Psychoacoustic characterization of the tinnitus spectrum: implications for the underlying mechanisms of tinnitus. Audiol. Neurootol. 7 (6), 358–369.

Olde Dubbelink, K.T.E., Hillebrand, A., Stoffers, D., Deijen, J.B., Twisk, J.W.R., Stam, C. J., Berendse, H.W., 2014. Disrupted Brain Network Topology in Parkinson's Disease: A Longitudinal Magnetoencephalography Study.

Pandit, A.S., Expert, P., Lambiotte, R., Bonnelle, V., Leech, R., Turkheimer, F.E., Sharp, D.J., 2013. Traumatic brain injury impairs small-world topology. Neurology 80 (20), 1826–1833. http://dx.doi.org/10.1212/WNL.0b013e3182929f38.

Pascual-Marqui, R.D., 2002. Standardized low-resolution brain electromagnetic tomography (sLORETA): technical details. Methods Find. Exp. Clin. Pharmacol. 24 (Suppl D), 5–12.

Rombach, M., Porter, M., Fowler, J., Mucha, P., 2014. Core-periphery structure in networks. SIAM J. Appl. Math. 74 (1), 167–190. http://dx.doi.org/10.1137/120881683.

Rubinov, M., Sporns, O., 2010a. Complex network measures of brain connectivity: uses and interpretations. NeuroImage 52 (3), 1059–1069.

Rubinov, M., Sporns, O., 2010b. Complex network measures of brain connectivity: uses and interpretations. NeuroImage 52 (3), 1059–1069. http://dx.doi.org/10.1016/j.neuroimage.2009.10.003.

Schlee, W., Mueller, N., Hartmann, T., Keil, J., Lorenz, I., Weisz, N., 2009. Mapping cortical hubs in tinnitus. BMC Biol. 7, 80. http://dx.doi.org/10.1186/1741-7007-7-80.

Senden, M., Deco, G., de Reus, M.A., Goebel, R., van den Heuvel, M.P., 2014. Rich club organization supports a diverse set of functional network configurations. NeuroImage 96, 174–182.

Song, J.J., De Ridder, D., Schlee, W., Van de Heyning, P., Vanneste, S., 2013a. "Distressed aging": the differences in brain activity between early- and late-onset tinnitus. Neurobiol. Aging. http://dxdoi.org/10.1016/j.neurobiolaging.2013.01.014.

Song, J.J., Punte, A.K., De Ridder, D., Vanneste, S., Van de Heyning, P., 2013b. Neural substrates predicting improvement of tinnitus after cochlear implantation in

patients with single-sided deafness. Hear. Res. 299, 1–9.
Sporns, O., 2013. Network attributes for segregation and integration in the human brain. Curr. Opin. Neurobiol. 23 (2), 162–171.
Sporns, O., Zwi, J.D., 2004. The small world of the cerebral cortex. Neuroinformatics 2 (2), 145–162. http://dx.doi.org/10.1385/NI:2:2:145.
Sporns, O., Chialvo, D.R., Kaiser, M., Hilgetag, C.C., 2004. Organization, development and function of complex brain networks. Trends Cogn. Sci. 8 (9), 418–425.
Stam, C.J., 2014. Modern network science of neurological disorders. Nat. Rev. Neurosci. 15 (10), 683–695. http://dx.doi.org/10.1038/nrn3801.
Stam, C.J., 2010. Use of magnetoencephalography (MEG) to study functional brain networks in neurodegenerative disorders. J. Neurol. Sci. 289 (1-2), 128–134. http://dx.doi.org/10.1016/j.jns.2009.08.028.
Stam, C.J., Jones, B.F., Nolte, G., Breakspear, M., Scheltens, P., 2007. Small-world networks and functional connectivity in Alzheimer's disease. Cereb. Cortex 17 (1), 92–99. http://dx.doi.org/10.1093/cercor/bhj127.
Stam, C.J., de Haan, W., Daffertshofer, A., Jones, B.F., Manshanden, I., van Cappellen, van Walsum, A.M., … Scheltens, P., 2009. Graph theoretical analysis of magnetoencephalographic functional connectivity in Alzheimer's disease. Brain 132 (Pt 1), 213–224. http://dx.doi.org/10.1093/brain/awn262.
Strogatz, S.H., 2001. Exploring complex networks. Nature 410 (6825), 268–276.
van den Heuvel, M.P., Sporns, O., 2011. Rich-club organization of the human connectome. J. Neurosci. 31 (44), 15775–15786. http://dx.doi.org/10.1523/JNEUROSCI.3539-11.2011.
van den Heuvel, M.P., Sporns, O., 2013. An anatomical substrate for integration among functional networks in human cortex. J. Neurosci. 33 (36), 14489–14500.
Vanneste, S., De Ridder, D., 2011a. Bifrontal transcranial direct current stimulation modulates tinnitus intensity and tinnitus-distress-related brain activity. Eur. J. Neurosci. 34 (4), 605–614. http://dx.doi.org/10.1111/j.1460-9568.2011.07778.x.
Vanneste, S., De Ridder, D., 2011b. The use of alcohol as a moderator for tinnitus-related distress. Brain Topogr. . http://dx.doi.org/10.1007/s10548-011-0191-0
Vanneste, S., Plazier, M., Ost, J., van der Loo, E., Van de Heyning, P., De Ridder, D., 2010a. Bilateral dorsolateral prefrontal cortex modulation for tinnitus by transcranial direct current stimulation: a preliminary clinical study. Exp. Brain Res. 202 (4), 779–785. http://dx.doi.org/10.1007/s00221-010-2183-9.
Vanneste, S., Plazier, M., Van Der Loo, E., Ost, J., Van de Heyning, P., De Ridder, D., 2010b. Burst transcranial magnetic stimulation: which tinnitus characteristics influence the amount of transient tinnitus suppression? Eur. J. Neurol. 17 (9), 1141–1147. http://dx.doi.org/10.1111/j.1468-1331.2010.02987.x.
Vanneste, S., Plazier, M., van der Loo, E., Van de Heyning, P., De Ridder, D., 2010c. The differences in brain activity between narrow band noise and pure tone tinnitus. PLoS One 5 (10), e13618. http://dx.doi.org/10.1371/journal.pone.0013618.
Vanneste, S., Plazier, M., van der Loo, E., Van de Heyning, P., De Ridder, D., 2011a. The difference between uni- and bilateral auditory phantom percept. Clin. Neurophysiol. 122 (3), 578–587.
Vanneste, S., van de Heyning, P., De Ridder, D., 2011b. The neural network of phantom sound changes over time: a comparison between recent-onset and chronic tinnitus patients. Eur. J. Neurosci. 34 (5), 718–731. http://dx.doi.org/10.1111/j.1460-9568.2011.07793.x.
Vecchio, F., Miraglia, F., Curcio, G., Della Marca, G., Vollono, C., Mazzucchi, E., … Rossini, P.M., 2015. Cortical connectivity in fronto-temporal focal epilepsy from EEG analysis: A study via graph theory. Clin. Neurophysiol. 126 (6), 1108–1116. http://dx.doi.org/10.1016/j.clinph.2014.09.019.
Watts, D.J., 1999. Networks, dynamics, and the small-world phenomenon. Am. J. Sociol. 105 (2), 493–527. http://dx.doi.org/10.1086/210318.
Watts, D.J., Strogatz, S.H., 1998. Collective dynamics of 'small-world' networks. Nature 393 (6684), 440–442. http://dx.doi.org/10.1038/30918.
Weisz, N., Moratti, S., Meinzer, M., Dohrmann, K., Elbert, T., 2005. Tinnitus perception and distress is related to abnormal spontaneous brain activity as measured by magnetoencephalography. PLoS Med. 2 (6), e153. http://dx.doi.org/10.1371/journal.pmed.0020153.
Wuchty, S., 2001. Scale-free behavior in protein domain networks. Mol. Biol. Evol. 18 (9), 1694–1702.
Yang, J., Leskovec, J., 2014. Overlapping Communities Explain Core-Periphery Organization of Networks.
Zhang, X., Martin, T., Newman, M.E.J., 2015. Identification of core-periphery structure in networks. Phys. Rev. E 91 (3), 032803.